

POLITECNICO DI MILANO

SCUOLA DI INGEGNERIA INDUSTRIALE E DELL'INFORMAZIONE

**CORSO DI LAUREA MAGISTRALE IN INGEGNERIA
MATEMATICA**



**ION ELECTRODIFFUSION FOR
CALCIUM DYNAMICS IN MYOCYTES**

RELATORE

Prof. Riccardo Sacco

CORRELATORI

Dr. Matteo Porro

Dr. Paola Causin

TESI DI LAUREA DI:

Elisa Pirovano

MATR. 787187

Anno Accademico 2013-2014

Abstract

Intracellular Ca^{2+} dynamics is a field of basic research in biology since Calcium signaling determines the functional behaviour of the principal cells in the body, including those of the nervous system and of the heart. To better understand the intracellular processes involving Ca^{2+} distributions it is necessary to distinguish the different intracellular compartments, since Calcium concentration is not uniform but may undergo important variations between different regions. This study provides a continuum-based mathematical model able to describe the main cell compartments of a myocyte, focusing on the dynamics of Calcium ion exchange between these compartments. Ion channels are modeled through suitable transmission conditions representing in a realistic manner ion flow across the membranes separating the various cell compartments. Numerical computations are performed in axisymmetric configurations, using an exponentially fitted finite element discretization adapted to treat these particular geometries. Simulation results reproduce in a biophysically accurate way the spatial and temporal Calcium distribution in the different cell regions using parameters based largely on experimental measurements in myocytes.

Abstract

Lo studio delle dinamiche della concentrazione intracellulare del Ca^{2+} è un ambito di ricerca fondamentale della biologia dal momento che il segnale del Calcio determina il comportamento funzionale delle principali cellule nel corpo, incluse quelle del sistema nervoso e del cuore. Per meglio comprendere i processi intracellulari che influenzano la distribuzione di Ca^{2+} è necessario distinguere i vari compartimenti all'interno della cellula poichè la concentrazione del Calcio libero non è uniforme ma può subire variazioni significative tra le differenti regioni. Questo studio fornisce un modello matematico in grado di descrivere in modo continuo i principali compartimenti cellulari di un miocita, ponendo particolare attenzione alle dinamiche di scambio di ioni Ca^{2+} tra di essi. I canali ionici sono modellati con opportune condizioni di trasmissione che rappresentano realisticamente il flusso di ioni attraverso le membrane che separano i vari compartimenti cellulari. Successivamente è stata introdotta una discretizzazione del modello matematico basata su un metodo ad elementi finiti di tipo exponential fitting, adattata per trattare le particolari configurazioni assialsimmetriche studiate. Le simulazioni condotte riproducono, in modo accurato dal punto di vista biofisico, la distribuzione spaziale e temporale di Calcio nelle diverse regioni della cellula con l'uso di parametri basati sulle misurazioni sperimentali nei miociti per la modellizzazione dei canali ionici.

*... Alla mia bisnonna Paola
per avermi cresciuta...*

Contents

1	Calcium dynamics : biological background	3
1.1	Calcium regulatory network	4
1.1.1	Characterization of Ca^{2+} fluxes	6
1.2	The cardiac myocyte: a review of fundamental concepts	6
1.3	Cellular Modelling	9
2	Mathematical Model	12
2.1	Geometrical representation of the cell	12
2.2	The PNP model for Calcium dynamics	14
2.2.1	Boundary conditions for the PNP model	20
3	Numerical Approximation	25
3.1	Linearization methods	25
3.1.1	Temporal discretization	26
3.2	PNP solution map	27
3.2.1	The Nonlinear Poisson equation	29
3.2.2	Continuity equations	29
3.3	Spatial discretization	31
4	Numerical simulations and results	36
4.1	Stationary simulations	36
4.1.1	Models for Calcium in the sarcoplasmic reticulum	37
4.2	Time dependent simulations	47
5	Conclusions and Future Work	51
A	The PNP system in scaled form	53
	Bibliography	59

List of Figures

1.1	Ca ²⁺ fluxes that drive the changes in Calcium concentration within different compartments	5
1.2	Longitudinal cross section of an individual cardiac myocyte	7
1.3	Structure of the sarcomere	8
1.4	Schematic representation of the alignment between myofibrils and SR membrane domains	9
1.5	A schematic description of the processes regulating uterine cell contraction (Taken from [2])	10
2.1	Cardiac myocyte composed of myofibrils, each of which contains myofilaments	13
2.2	Geometry of the cell	14
2.3	Microscale model of the sarcoplasmic reticulum: 1D cross-section of the cellular domain.	17
2.4	Geometry of the cell after model reduction	18
3.1	PNP solution map	30
3.2	Partition of the computational domain Ω into two different but communicating parts	32
4.1	Mesh for the axisymmetric geometry of Fig.2.2: the blue grid represents the subdomain Ω_1 , the red represents Ω_2	38
4.2	Concentrations	41
4.3	Calcium concentration in the sarcoplasmic reticulum computed using model (4.1) for the SR	42
4.4	Calcium concentration in the sarcoplasmic reticulum computed using model (4.3) for the SR and setting $m_1=740$ and $m_2=0.9$	43
4.5	Concentrations	44
4.6	Concentrations trend due to the variation of the parameter m_1	45
4.7	Intracellular potential	45

4.8	Component of the two fluxes \mathbf{f}_1 and \mathbf{f}_2 computed using model (4.3) for the SR and setting $m_1=740$ and $m_2=0.9$	46
4.9	SR Ca Pump flux	48
4.10	Na-Ca exchanger flux	50

List of Tables

2.1	SR Ca pump parameters	22
2.2	SL Ca pump parameters	24
2.3	Na-Ca exchange parameters	24
4.1	Environmental parameters	39
4.2	Calcium average concentrations	47

Introduction

The subject matter of the present research is the dynamics of a specific signaling ion, which controls the functional responses in a wide variety of cells: the ionized free Calcium. Calcium is responsible for different cell activities, like smooth muscle cell contraction, channel expressions and cell proliferation. Calcium dynamics is principally, although not exclusive, regulated by the membrane potential, because of the characteristic of the cell membrane which contains many proteins like channels, pumps and Na-Ca exchangers. The complexity of Calcium dynamics is also influenced by cell compartments each of which is characterized by a distinct mode of regulation. For these reasons the understanding of Calcium dynamics requires the knowledge of the different cell compartments and of the transport mechanisms which regulate the Calcium fluxes between the compartments. In order to develop a mathematical model of intracellular Calcium dynamics, it has been first necessary to define a geometrical model of the cell, which takes into account the various compartments involved in the dynamics of Calcium ions. Then, on this geometry we have proposed a system of partial differential equations to calculate the intracellular concentration and the Calcium fluxes across the membrane. Finally, numerical computations based on the use of the finite element method, have been carried out to validate the model against physiological evidence.

The structure of the thesis consists in a first chapter in which we describe the role

of Calcium in cells and its dynamics. Successively, we consider the case of myocytes, involved in the mechanical function of the heart, and we describe the cell structure focusing on the main structural components responsible for the propagation of calcium ions into the cell.

Following this biological background, in Chapter 2 we introduce the geometrical model which takes into account the different parts of the cell, and we build up the mathematical model for Calcium electrodiffusion based on the Poisson-Nernst-Planck system of partial differential equations supported by appropriate initial and boundary conditions. We choose the boundary conditions in order to properly reproduce ion fluxes considering the dynamics of the different proteins present on the plasma membrane and intracellular interface.

In Chapter 3 we introduce the numerical methods implemented to solve the mathematical model. Time dependence is treated using the Backward Euler scheme and at each time level the resulting nonlinear system is solved with the Gummel Map iterative procedure. Finally, to test the mathematical and numerical model, in Chapter 4 we simulate the Calcium spatial distributions inside the distinct subdomains in the stationary case, introducing two different models for the Calcium concentration in the SR. Then we introduce the time dependence of the continuity equations in order to reproduce the behaviour of ion channels located on the membranes of the cell and we compare the obtained results with previous studies. Simulations are in both stationary and time-dependent regimes in good accordance between biophysical expectations and results published in the specialized literature.

Chapter 1

Calcium dynamics : biological background

Ionized free Calcium, Ca^{2+} , is a widespread signaling ion that serves as both charge carrier and chemical intermediate linking many physiological stimuli to their intracellular effectors. Calcium controls directly or indirectly long-term responses in cells, including release of endothelium-derived hyperpolarizing and relaxing factor, smooth muscle cell (SMC) contraction, channel expression and cell proliferation.

As shown by studies of Friel et al. [5], Ca^{2+} is closely regulated by membrane potential, which is also an important intracellular signal. Because of the complexity of cellular Ca^{2+} signaling, it is difficult to predict how natural stimuli or pharmacological perturbations affect Calcium levels and thus the ultimate effects of Calcium on cell functions such as membrane excitability, protein phosphorylation and gene regulation. Ca^{2+} acts by binding to specific receptor sites whose occupancy translates the Ca^{2+} signal into downstream cellular effects. Calcium dynamics represents the key link between stimulus and response, so that the binding sites occupancy depends on Calcium concentration itself. Ca^{2+} concentration

is regulated by channels, pumps, exchangers and buffers that determine the relationship between the levels of free and bound Calcium. Some buffers directly transduce Ca^{2+} signals, while others act indirectly by binding Ca^{2+} and modifying its signal received by buffers of the first type.

1.1 Calcium regulatory network

Cell compartments and organelles, like cytoplasm, mitochondria and endoplasmic reticulum, influence the complexity of Ca^{2+} dynamics, because each of them is characterized by distinct Ca^{2+} sensitive processes and mode of regulation. Within each compartment of the cell the Calcium concentration changes at a rate that depends on the net Ca^{2+} flux entering the compartment volume. Thus it is important to understand the mechanisms used by each compartment to handle Ca^{2+} flux and regulate its internal Calcium levels. The depolarization of the cell membrane initiates Calcium ion entry into cells through voltage-operated Ca^{2+} channels (VOCCs) and thereby a rise in the intracellular Ca^{2+} concentration. The elevated level of Ca^{2+} inside the cell allows binding of Ca^{2+} and calmodulin, a Calcium binding messenger protein, thus activating myosin light-chain kinase, which phosphorylates a regulatory myosin light chain. This subsequently allows the formation of cross bridges between actin and myosin filaments and the generation of muscle contraction. Each macroscopic Ca^{2+} flux through the different membrane channels, influences the Ca^{2+} concentration which, in turn, influences other Ca^{2+} handling sites. The Ca^{2+} transport pathways that regulate Ca^{2+} concentration in each compartment depend on Ca^{2+} dynamics in the other compartments. As a result, Ca^{2+} dynamics in all of these compartments are functionally and naturally coupled, so that, understanding Ca^{2+} dynamics within a given compartment requires understanding the Ca^{2+} handling system used by that compartment to reg-

ulate its internal Ca^{2+} levels. In order to address the study of Ca^{2+} dynamics we consider the example taken from [5] and illustrated in Figure 1.1. The net Ca^{2+} flux that drives changes in Calcium concentration, henceforth denoted by $[\text{Ca}^{2+}]_i$, within the cytosol depends on Ca^{2+} transport across the plasma membrane and between the cytoplasm and organelles such as mitochondria and the Endoplasmic reticulum. This exchange of mass is denoted by the fluxes J_{PM} , J_{MT} and J_{ER} . Each intercompartmental Ca^{2+} flux is the sum of multiple macroscopic Ca^{2+} fluxes that represent the activity of specific populations of Ca^{2+} transporters. For example the flux across the plasma membrane would include contributions from Ca^{2+} entry through voltage-sensitive channels and leak channels, and Ca^{2+} export via Na/Ca exchangers and other pathways.

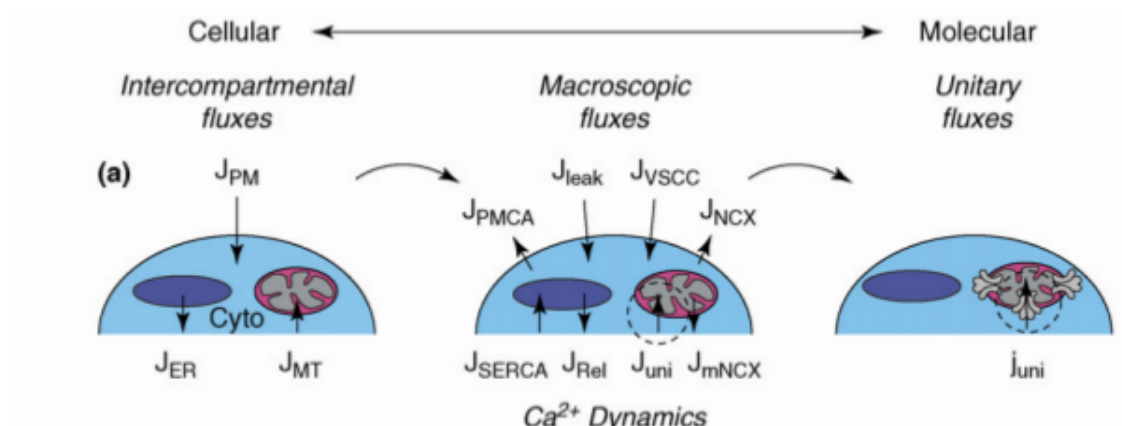


Figure 1.1: Ca^{2+} fluxes that drive the changes in Calcium concentration within different compartments

Understanding Ca^{2+} dynamics requires the knowledge of the distinct cellular compartments that participate in the Ca^{2+} regulatory network, the relationship between free and total Ca^{2+} concentrations in these compartments, and ultimately, of Ca^{2+} transport system which regulates the net flux of Ca^{2+} between compartments and the rate laws governing their operation.

1.1.1 Characterization of Ca^{2+} fluxes

In [5] an approach is shown to measure Ca^{2+} fluxes across the plasma membrane. These fluxes include contributions from plasma membrane Ca ATPases, Na/Ca exchangers and possibly other unknown transporters operating in parallel with inward Ca^{2+} leak. These pathways can be lumped together to give an overall description of surface-membrane Ca^{2+} transport in the absence of stimulation. The overall rate of Ca^{2+} transport is the sum of the macroscopic Ca^{2+} flux components and increases with internal Ca^{2+} concentration. Because the direction of this net flux is outward when $[\text{Ca}^{2+}]_i$ is above the resting level, where the component fluxes are in balance, we call it 'extrusion', while net transport is inward when $[\text{Ca}^{2+}]_i$ is below the resting level.

1.2 The cardiac myocyte: a review of fundamental concepts

In order to develop a geometrical and mathematical model of calcium dynamics we focus our research on a specific cell type, the cardiac myocyte. The myocardium is an organized tissue, composed of several cell types that include smooth muscle cells, fibroblasts and cardiac myocyte. The fundamental contractile cell of the myocardium is the myocyte and we now briefly examine its main structural components. In this section we give a brief description of the main components of a myocyte and we refer to [10], [15], [12] for a more detailed treatment. An illustration of the organization of the structures of the cardiac myocyte is shown in Figure 1.2. The myocyte is composed of bundles of myofibrils that contain myofilaments. Myofibrils are composed of repeating sections of sarcomeres which are composed of long, fibrous proteins that slide past each other

when the muscles contract and relax. Two of the important proteins are myosin, which forms the thick filament, and actin, which forms the thin filament and actin molecules are bound to the Z line, which forms the borders of the sarcomere (Figure 1.3). The sarcomere is the repeating unit of cardiac myocyte, thus to understand how does it work, we need to understand the structure and function of a single sarcomere.

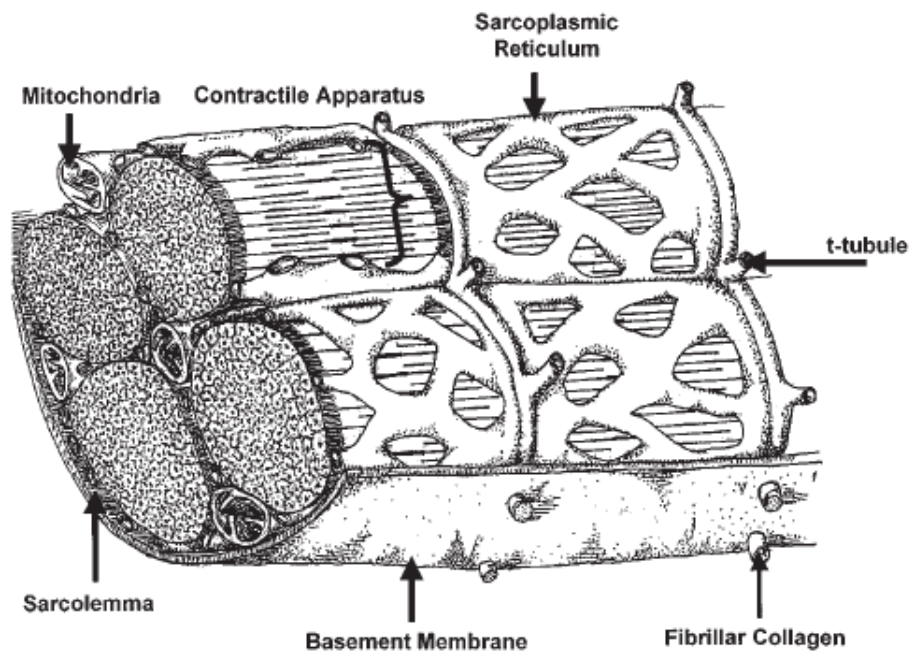


Figure 1.2: Longitudinal cross section of an individual cardiac myocyte

The first important component of a myocyte is the sarcolemma, a specialized structure of the myocyte composed of a lipid bilayer which contains hydrophilic heads and hydrophobic tails. This configuration allows the sarcolemma to interact with the intracellular and extracellular environments. The fundamental function of sarcolemma is to provide a barrier for diffusion. It also contains membrane proteins, which include receptor, pumps and channels. A specialized feature of

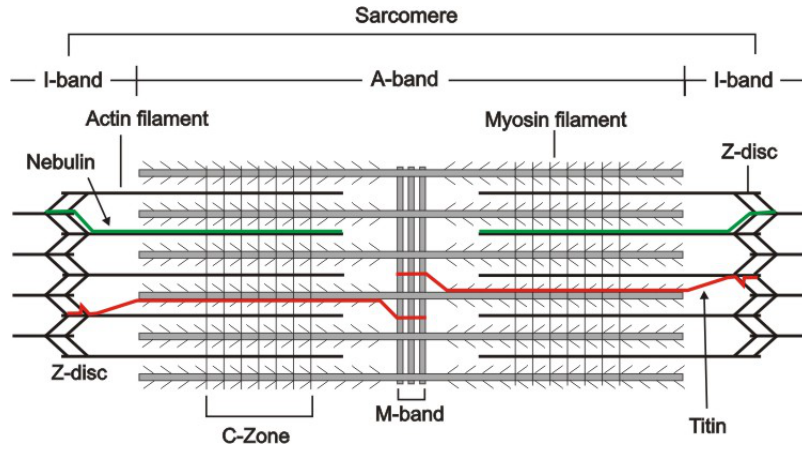


Figure 1.3: Structure of the sarcomere

the sarcolemma is its essential role in the contractile process of the myocyte described in Section 1.1. The other important component in developing our model is the sarcoplasmic reticulum (SR), an intracellular membrane network which is a highly efficient Ca^{2+} handling organelle, specialized in the regulation of cytosolic Ca^{2+} concentration. The SR can be divided into at least two domains, the longitudinal SR and the junctional SR. The first one is composed of numerous tubules interconnected with each other forming a network around each myofibril, the contractile unit of the myocyte. At their ends, the longitudinal tubules coalesce into a single dilated sac called terminal cisterna. Both the longitudinal and the junctional SR show a specific spatial organization with respect to the myofibrils. Figure 1.4 illustrates the distribution of SR domains around each sarcomere.

The sarcoplasmic reticulum, responsible for the Ca^{2+} source in excitation contraction coupling, contains three important components that participate in the role of this organelle with respect to Ca^{2+} homeostasis: the SR Ca^{2+} ATPase, phospholamban and the Ca^{2+} release channels. In [13] the Calcium transport out of the SR into the cytosol was calculated as the difference of two fluxes:

$$J_{\text{SR}} = J_{\text{rel}} - J_{\text{pump}}$$

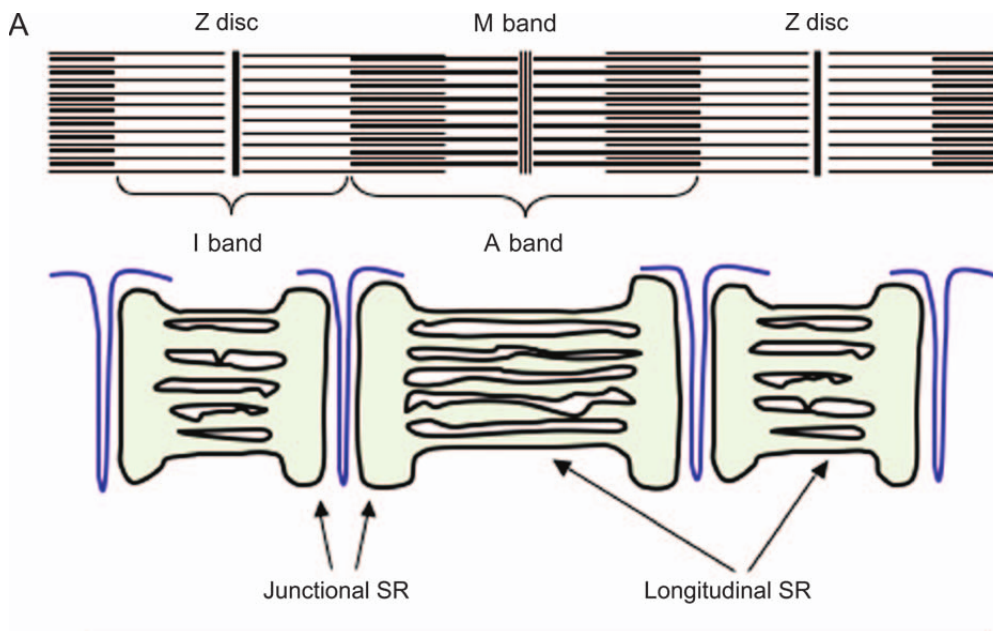


Figure 1.4: Schematic representation of the alignment between myofibrils and SR membrane domains

where J_{rel} is the SR Calcium release flux and J_{pump} is the SR Calcium pump flux. The SR Calcium pump is found only in the cytosolic portion of the membrane, that accounts for 90% of the total cell membrane, and the flux J_{pump} depends on Calcium concentration on both sides of the SR membrane.

1.3 Cellular Modelling

The majority of the studies in literature, [2], [3], [13], [12], [7], [14], use multi-compartmental models for cell modeling. A multi-compartment model is a mathematical framework describing how substances are transmitted among the compartments of a system. Each compartment is assumed to be a homogeneous entity within which the quantities being modelled are uniformly distributed, hence a multi-compartment model is a lumped parameter model. A significant example is reported in [2], where the biophysics of excitation-contraction in a uterine my-

ocyte is described with three simultaneous processes (see Figure 1.5).

In the first process it is assumed that Ca^{2+} enters the cell in response to membrane depolarization, in the second process two mechanisms of Ca^{2+} extrusion out of the cell are assumed: Ca^{2+} pumps and $\text{Na}^+ / \text{Ca}^{2+}$ exchangers across the plasma membrane. Finally the third process describes the myocyte contraction.

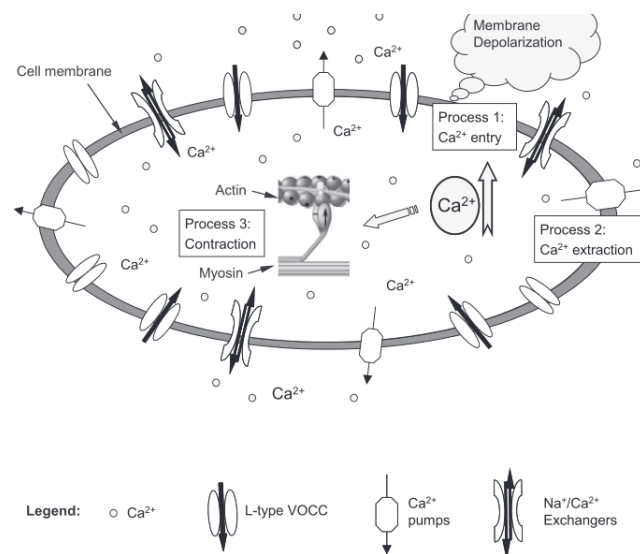


Figure 1.5: A schematic description of the processes regulating uterine cell contraction (Taken from [2])

Another approach, proposed in [13], includes the subsarcolemma compartment along with the junctional and bulk cytosolic compartments to allow proteins in the membrane to sense ion concentrations that differ from those in the bulk. The cell is separated into four lumped compartments: the sarcoplasmic reticulum, the junctional cleft, the subsarcolemma space and the bulk cytosolic space. The goal of the analysis in [13] is to track ion influx and efflux such that the model reaches a steady state with a realistic balance of Calcium fluxes, to incorporate a form of

Ca-induced Ca release and to simulate basic physiological phenomena when all the components are combined, with realistic parameters that are consistent with laboratory observations.

Starting from [13] we want to develop a cellular model based on a continuum approach. In [8] an approach is proposed to extend the traditional compartmental models in order to obtain a continuum based formulation. A highly refined 2-D spatial resolution within cytosol and microdomains can be achieved with the finite element method approach. Based on the compartmental models the authors of [8] have implemented SMC models in 2-D rectangular and cylindrical domains, with 2D axial symmetry. They calculate the intracellular and extracellular concentrations of different ionic species, with the time-dependent electrodiffusion Nernst-Planck equations coupled with the electroneutrality condition.

Based on all of these studies we want to introduce a new geometrical model for the cell, which takes into account the different parts of the intracellular environment. On this geometry we want to implement a system of partial differential equations (PDEs) in order to calculate the intracellular Calcium concentration with time-dependent electrodiffusion equations as in [8]. We also want to use the equations proposed in [13] for the Calcium fluxes across the different membranes, as boundary conditions for our continuum model.

Chapter 2

Mathematical Model

In this chapter we discuss the geometry used to represent the cell and the equations used to mathematically describe the intracellular distribution of the different ions and the evolution of the membrane potential. Based on the studies of Shannon et al. in [12, 13], we apply our mathematical description to a specialized muscle cell, the cardiac myocyte. For this purpose we consider the Poisson-Nernst-Planck system of partial differential equations for ion electrodiffusion supported by suitable boundary and initial conditions.

2.1 Geometrical representation of the cell

As suggested in Figure 2.1, the cardiac myocyte has a stretched form and can be geometrically approximated as a cylinder. For sake of simplicity we consider the cell as constituted by a single sarcomere, therefore the sarcoplasmic reticulum is located below the cell membrane, which is represented by the lateral surface of the cylinder, and entirely wraps the inside region of the sarcomere, consisting of the cytosol. In the present study, we consider the sarcoplasmic reticulum as a continuous surface, although it is characterized by a dense network.

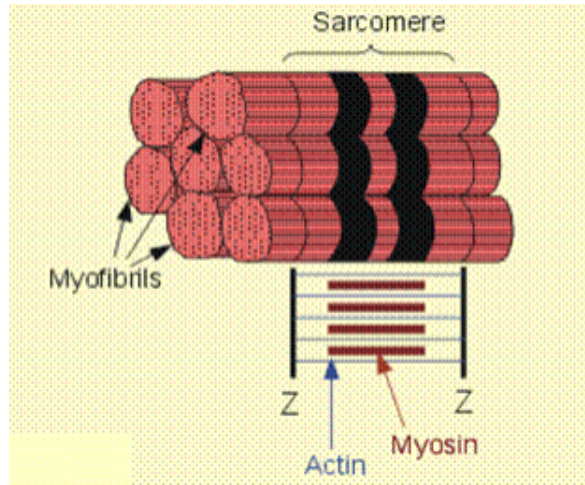


Figure 2.1: Cardiac myocyte composed of myofibrils, each of which contains myofilaments

Subsequently we consider a two dimensional geometrical model of the cell, with an axisymmetric configuration. The cell looks like a small cylinder of radius $R = 1\mu m$ and height $L = 100\mu m$, the dependence on the ϕ -coordinate being neglected so that we can solve the mathematical problem in the plane (r, z) , obtaining the three dimensional model with a rotation of such a plane around the symmetry axis (Figure 2.2).

Considering the 2D geometrical representation of the cell, we divide the rectangular domain Ω in three subdomains Ω_1 , Ω_2 and Ω_{SR} , which represent the cytosolic space, the subsarcolemma space and the sarcoplasmic reticulum of the cell, respectively. We can also distinguish three different boundaries in the two subdomains:

1. Γ_l and Γ_r which represent the left and right junctional membranes of the cell, where about 90 % of the L-type calcium channels is concentrated;
2. Γ_s , which represents the sarcolemma.

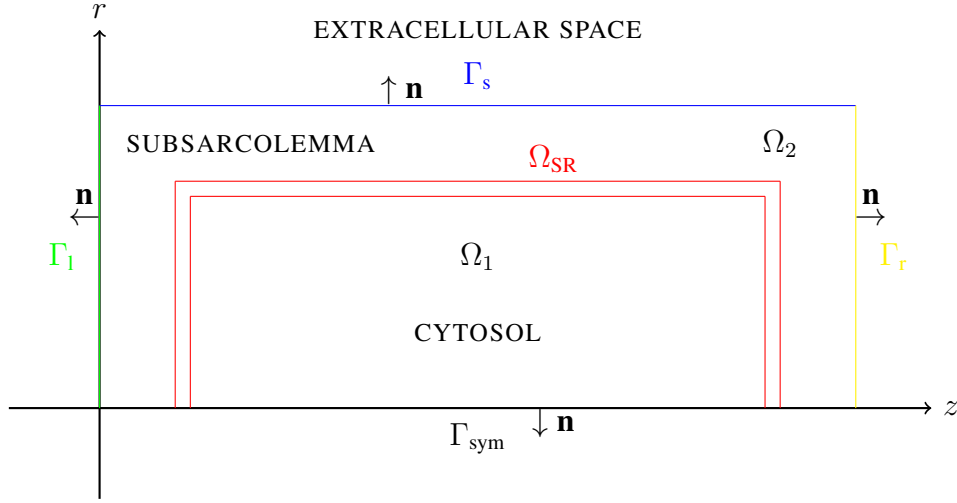


Figure 2.2: Geometry of the cell

We notice that from the point of view of geometrical representation, the physical domain boundaries Γ_l , Γ_r and Γ_s are treated as one dimensional manifolds, thereby neglecting their actual thickness.

2.2 The PNP model for Calcium dynamics

In this section we illustrate the mathematical model to study the dynamics of Calcium inside the cell, in view of describing the excitation-contraction coupling in muscle cells. We consider four different variables:

- c_1 , the concentration of Calcium in the subdomain Ω_1 , which represents the amount of Calcium inside the cytosolic compartment;
- c_2 , the concentration of Calcium in the subdomain Ω_2 , which represents the amount of Calcium in the subsarcolemma space;
- c_{SR} , the concentration of Calcium along the one dimensional manifold Γ_{SR} , which represents the amount of Calcium in the sarcoplasmic reticulum;

- φ , the membrane potential of the muscle cell.

To describe Calcium electrodiffusion inside the cell volume, we use the Poisson-Nernst-Planck model (see [11]). This amounts to solving the following four differential problems with the associated boundary and initial conditions.

The first problem is for the dependent variable c_1 to be solved in the subdomain Ω_1 :

$$\frac{\partial c_1}{\partial t} + \operatorname{div} \mathbf{f}_1 = 0 \quad (2.1a)$$

$$\mathbf{f}_1 = z\mu c_1 \mathbf{E} - D\nabla c_1 \quad (2.1b)$$

$$\mathbf{f}_1 \cdot \mathbf{n}_1 = J_{\text{SR}}^1 \quad \text{on } \Gamma_{\text{SR}} \quad (2.1c)$$

$$\mathbf{f}_1 \cdot \mathbf{n} = 0 \quad \text{on } \Gamma_{\text{sym}} \cap \partial\Omega_1 \quad (2.1d)$$

$$c_1(\mathbf{x}, 0) = c_1^0(\mathbf{x}) \quad \text{in } \Omega_1 \quad (2.1e)$$

The second problem consists in finding the dependent variable c_2 by solving the following equations in Ω_2 :

$$\frac{\partial c_2}{\partial t} + \operatorname{div} \mathbf{f}_2 = 0 \quad (2.2a)$$

$$\mathbf{f}_2 = z\mu c_2 \mathbf{E} - D\nabla c_2 \quad (2.2b)$$

$$\mathbf{f}_2 \cdot \mathbf{n} = J_{\text{NCX}} + J_{\text{pump}} \quad \text{on } \Gamma_s \quad (2.2c)$$

$$\mathbf{f}_2 \cdot \mathbf{n} = J_{\text{junction}} \quad \text{on } \Gamma_l \quad (2.2d)$$

$$\mathbf{f}_2 \cdot \mathbf{n} = J_{\text{junction}} \quad \text{on } \Gamma_r \quad (2.2e)$$

$$\mathbf{f}_2 \cdot \mathbf{n}_2 = J_{\text{SR}}^2 \quad \text{on } \Gamma_{\text{SR}} \quad (2.2f)$$

$$\mathbf{f}_2 \cdot \mathbf{n} = 0 \quad \text{on } \Gamma_{\text{sym}} \cap \partial\Omega_2 \quad (2.2g)$$

$$c_2(\underline{\mathbf{x}}, 0) = c_2^0(\underline{\mathbf{x}}) \quad \text{in } \Omega_2 \quad (2.2h)$$

The variable c_{SR} is determined by solving in Ω_{SR} the following equation

$$\frac{\partial c_{\text{SR}}}{\partial t} + \operatorname{div} \mathbf{f}_{\text{SR}} = P_{\text{SR}}(c_1, c_2, c_{\text{SR}}) \quad (2.3)$$

where P_{SR} is the net production rate in Ω_{SR} , depending in general on c_1 , c_2 and c_{SR} . Since the thickness of the domain Ω_{SR} , t_{SR} , is such that $t_{\text{SR}} \ll l_{ch}$, where l_{ch} is the characteristic length of the domain Ω , a geometrical and functional model reduction is in order. The flux inside the domain Ω_{SR} is defined as

$$\mathbf{f}_{\text{SR}} = \mathbf{v}_{\text{SR}} c_{\text{SR}}$$

where \mathbf{v}_{SR} is the total velocity acting on c_{SR} , which in general includes both advective and diffusive contributions. For simplicity, in this analysis we assume $\mathbf{v}_{\text{SR}} = 0$ and therefore the resulting flux is null. In order to introduce the 1-dimensional manifold Γ_{SR} , corresponding to the middle crosssection of the SR volume Ω_{SR} , we have to average the equation for the variable c_{SR} in this domain. Referring

to to Figure 2.3 we integrate our equation for the variable c_{SR} in the ξ -direction, where $\xi = r, z$ depending on the considered region of the SR, and we obtain:

$$\int_{-\frac{t_{\text{SR}}}{2}}^{\frac{t_{\text{SR}}}{2}} \frac{\partial c_{\text{SR}}}{\partial t} d\xi = \int_{-\frac{t_{\text{SR}}}{2}}^{\frac{t_{\text{SR}}}{2}} P_{\text{SR}}(c_1, c_2, c_{\text{SR}}) d\xi \quad \text{in } \Omega_{\text{SR}} \quad (2.4)$$

which is equivalent to

$$\frac{\partial \langle c_{\text{SR}} \rangle}{\partial t}(t, \xi) = \langle P_{\text{SR}} \rangle \quad \text{in } \Gamma_{\text{SR}} \quad (2.5)$$

where $\langle u \rangle$ is the spatial average of u along the coordinate ξ . For future purposes, we replace $\langle c_{\text{SR}} \rangle$ and $\langle P_{\text{SR}} \rangle$ with their values at each point (r, z) of the mid section of Ω_{SR} and we replace Ω_{SR} with its geometrical mid-section axis, the one-dimensional manifold Γ_{SR} (see Figure 2.4).

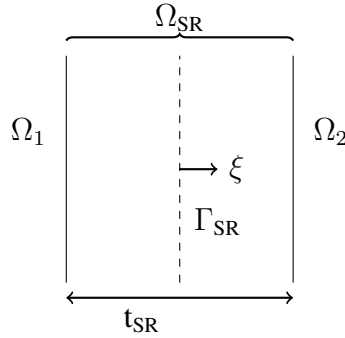


Figure 2.3: Microscale model of the sarcoplasmic reticulum: 1D cross-section of the cellular domain.

The concentrations c_1 , c_2 and c_{SR} are measured in [mM], equal to $[\text{mol}][\text{m}]^{-3}$ and all the fluxes \mathbf{f}_i are expressed in $[\text{mM}][\text{m}][\text{s}]^{-1}$.

In the Nernst-Planck equations (2.1b) and (2.2b) for the ion fluxes, μ and D are electrical mobility and diffusivity, respectively. These latter quantities are related

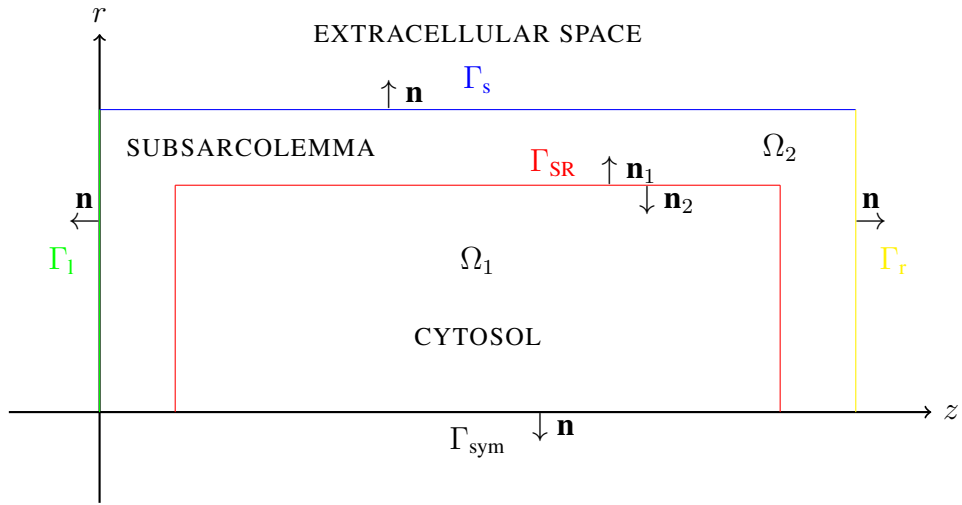


Figure 2.4: Geometry of the cell after model reduction

by the Einstein relation:

$$D = \frac{\mu V_{th}}{|z|} \quad (2.6)$$

where $V_{th} = \frac{K_b T}{q}$ is the thermal voltage, K_b is the Boltzmann constant, T the absolute temperature and q is the elementary charge.

Finally to close the problem we have to solve the following Poisson equation in Ω_1 and Ω_2 :

$$\operatorname{div} \mathbf{D} = \rho_{\text{mob}} + \rho_{\text{fix}} \quad \text{in } \Omega_i \quad i = 1, 2 \quad (2.7a)$$

$$\mathbf{D} = -\epsilon \nabla \varphi \quad \text{in } \Omega_i \quad i = 1, 2 \quad (2.7b)$$

$$\mathbf{D} \cdot \mathbf{n} = 0 \quad \text{on } \Gamma_s \quad (2.7c)$$

$$\mathbf{D} \cdot \mathbf{n} = c_m(\varphi - V_l) \quad \text{on } \Gamma_l \quad (2.7d)$$

$$\mathbf{D} \cdot \mathbf{n} = c_m(\varphi - V_r) \quad \text{on } \Gamma_r \quad (2.7e)$$

$$[[\mathbf{D}]] = -\sigma_{\text{SR}} \quad \text{on } \Gamma_{\text{SR}} \quad (2.7f)$$

$$[[\varphi]] = 0 \quad \text{on } \Gamma_{\text{SR}} \quad (2.7g)$$

$$\mathbf{D} \cdot \mathbf{n}_{\text{sym}} = 0 \quad \text{on } \Gamma_{\text{sym}} \quad (2.7h)$$

The vector \mathbf{D} is the electric displacement defined as

$$\mathbf{D} = \epsilon \mathbf{E}$$

ϵ being the dielectric constant of the medium in which ion flow takes place and

$$\mathbf{E} = -\nabla \varphi$$

being the electric field experienced by the charged ions in motion throughout the medium.

The right-hand side in equation (2.7a) is the electric charge density

$$\rho = \rho_{\text{mob}} + \rho_{\text{fix}}$$

at each point of the cell and at each time level where ρ_{fix} is a fixed charge density accounting for the presence of other ions in the medium while ρ_{mob} is the mobile

charge density. The two charge densities are defined as

$$\rho_{\text{mob}_i} = 2qN_{\text{av}}c_i$$

$$\rho_{\text{fix}} = qN_{\text{av}} \sum_{j=1}^M z_j c_j$$

where q is the electric charge unit, N_{av} is Avogadro's constant and the subscript $i = 1, 2$ refers to the domain in which equation (2.7a) must be solved while M indicates the number of fixed charges present in the medium.

The units of \mathbf{D} , ρ and ϵ are $[\text{C}][\text{m}]^{-2}$, $[\text{C}][\text{m}]^{-3}$ and $[\text{F}][\text{m}]^{-1}$, respectively. The boundary conditions (2.7f), (2.7g) express transmission conditions on the internal boundary Γ_{SR} . In particular:

$$[[\mathbf{D}]] := \mathbf{D}_1 \cdot \mathbf{n}_1 + \mathbf{D}_2 \cdot \mathbf{n}_2$$

is the jump of \mathbf{D} across Γ_{SR} and \mathbf{D}_i is the restriction of the vector in the subdomain Ω_i , $i = 1, 2$.

In the same way we define the jump of the electric potential φ :

$$[[\varphi]] := \varphi_1 \cdot \mathbf{n}_1 + \varphi_2 \cdot \mathbf{n}_2$$

Finally c_m , V_l and V_r are the membrane capacitance, expressed in $[\text{F}][\text{m}]^{-1}$, and the external potential on the right and left sides of the cell respectively.

2.2.1 Boundary conditions for the PNP model

In this section we illustrate in more detail the different conditions imposed on each boundary of the two subdomains.

The interface between the two subdomains, labeled as Γ_{SR} , represents the sar-

coplasmic reticulum of the cell and for this reason we impose the condition (2.1c) in solving the first problem and (2.2f) for the second one. The right-hand side in (2.1c), J_{SR}^1 , is defined following the model proposed in [13]. It describes the behaviour of the SR Ca pumps that are found only in the cytosolic portion of the membrane that accounts for the 90% of the total membrane. The expression for J_{SR}^1 is

$$J_{\text{SR}}^1 = Q_{10\text{-SRCaP}} \frac{V_{\max} \left(\frac{c_1}{K_{\text{mf}}} \right)^H - V_{\max} \left(\frac{c_{\text{sr}}}{K_{\text{mr}}} \right)^H}{1 + \left(\frac{c_1}{K_{\text{mf}}} \right)^H + \left(\frac{c_{\text{sr}}}{K_{\text{mr}}} \right)^H} \frac{V_{\text{cytosol}}}{A_{\text{cytosol}}} \quad (2.8)$$

where V_{cytosol} and A_{cytosol} are the volume and the surface of the three dimensional domain which is obtained by rotating the subdomain Ω_1 around the symmetry, axis whose ratio is equal to

$$\frac{V_{\text{cytosol}}}{A_{\text{cytosol}}} = \frac{R_{\text{cytosol}} Z_{\text{cytosol}}}{2(R_{\text{cytosol}} + Z_{\text{cytosol}})}$$

where R_{cytosol} and Z_{cytosol} are the radius and the z-length of the subdomain Ω_1 , respectively.

Equation (2.8) can be written as

$$J_{\text{SR}}^1 = \alpha_{\text{SR}} c_1 - \beta_{\text{SR}} \quad (2.9)$$

upon defining

$$\alpha_{\text{SR}} = Q_{10\text{-SRCaP}} \frac{V_{\max} \left(\frac{c_1^{(\text{old})}}{K_{\text{mf}}} \right)^{H-1}}{1 + \left(\frac{c_1^{(\text{old})}}{K_{\text{mf}}} \right)^H + \left(\frac{c_{\text{sr}}^{(\text{old})}}{K_{\text{mr}}} \right)^H} \frac{V_{\text{cytosol}}}{A_{\text{cytosol}}}$$

$$\beta_{\text{SR}} = Q_{10\text{-SRCaP}} \frac{V_{\max} \left(\frac{c_{\text{sr}}^{(\text{old})}}{K_{\text{mr}}} \right)^H}{1 + \left(\frac{c_1^{(\text{old})}}{K_{\text{mf}}} \right)^H + \left(\frac{c_{\text{sr}}^{(\text{old})}}{K_{\text{mr}}} \right)^H} \frac{V_{\text{cytosol}}}{A_{\text{cytosol}}}$$

Parameters	Value	Units
V_{\max}	286	$[\mu\text{mol}][\text{l}_{\text{cytosol}}]^{-1}[\text{s}]^{-1}$
K_{mf}	0.246	$[\mu\text{M}]$
K_{mr}	1.7	$[\text{mM}]$
H	1.787	
k_s	25	$[\text{m}][\text{s}]^{-1}$
O	10^{-7}	
$Q_{10\text{-SRCaP}}$	2.6	

Table 2.1: Parameters used to define the flux J_{SR} across Γ_{SR}

In this way we have a Robin boundary condition for the problem (2.1a) - (2.1b), which is numerically implemented using the value of c_1 and c_{SR} at the previous step of our algorithm, in the definitions of α_{SR} and β_{SR} .

In the same way we can define a Robin boundary condition for the flux \mathbf{f}_2 across the interface Γ_{SR} . The expression of the flux (2.2f) is

$$J_{\text{SR}}^2 = k_s O(c_2 - c_{\text{SR}}) \quad (2.10)$$

which model the SR Calcium release channel.

The unit of the flux J_{SR}^i is $[\text{mM}][\text{m}][\text{s}]^{-1}$ and all the parameters in (2.8) and (2.10) are taken from [13] and are listed in Table 2.1.

In (2.2) we also have to define other three different conditions for the flux \mathbf{f}_2 . On Γ_s we consider two different contributions, because this part of the boundary represents the sarcolemma of the muscle cell on which we can find different transport proteins. We take into account the SL Ca Pumps and the Na-Ca exchangers

with these two fluxes

$$J_{\text{pump}} = -\frac{F x_{\text{SLCap}} Q_{\text{SLCap}} V_{\text{max}} V_{\text{cell}}}{1 + \left(\frac{K_m}{c_2}\right)^H} \frac{V_{\text{cell}}}{A_{\text{cell}}} \quad (2.11)$$

$$J_{\text{NCX}} = \frac{K_a Q_{\text{NCX}} V_{\text{max}} \left(\exp\left(\frac{\eta VF}{RT}\right) \text{Na}|_2^{\text{HNa}} c_{\text{out}} - \exp\left(\frac{(\eta-1)VF}{RT}\right) \text{Na}|_{\text{out}}^{\text{HNa}} c_2 \right)}{\left(\begin{array}{l} K_{\text{mCai}} \text{Na}|_{\text{out}}^{\text{HNa}} \left(1 + \left(\frac{\text{Na}|_2}{K_{\text{mNai}}}\right)^{\text{HNa}}\right) \\ + K_{\text{mNao}}^{\text{HNa}} c_2 \left(1 + \frac{c_2}{K_{\text{mCai}}}\right) + K_{\text{mCao}} \text{Na}|_2^{\text{HNa}} \\ + \text{Na}|_2^{\text{HNa}} c_{\text{out}} + \text{Na}|_{\text{out}}^{\text{HNa}} c_2 \end{array} \right) \left(1 + k_{\text{sat}} \exp\left(\frac{(\eta-1)VF}{RT}\right)\right)} \frac{V_{\text{cell}}}{A_{\text{cell}}} \quad (2.12)$$

where R , F and T are the ideal gas constant, the Faraday constant and the absolute temperature, respectively. V represents the potential drop outside the cell and

$$\frac{V_{\text{cell}}}{A_{\text{cell}}} = \frac{R_{\text{cell}} Z_{\text{cell}}}{2(R_{\text{cell}} + Z_{\text{cell}})}$$

is the ratio between the volume and the surface of the cell.

The parameters for the two fluxes (2.11) and (2.12) are listed in Table 2.2 and Table 2.3, respectively, while K_a depends on the dependent variable c_2 and is defined as

$$K_a = \frac{1}{1 + \left(\frac{K_{\text{d-Act}}}{c_2}\right)^3} \quad (2.13)$$

The two boundaries Γ_s and Γ_r represent the junctional membrane of the cell where the L-type Ca channels are concentrated. The formulation of the fluxes in these regions is based on the Goldman-Hodgkin-Katz (GHK) equation (see [9, 4] for more details)

$$J_{\text{junction}} = P_{Ca} \left[\text{Be} \left(-\frac{z(V_{\text{out}} - \varphi)}{V_{\text{th}}} \right) c_2 - \text{Be} \left(\frac{z(V_{\text{out}} - \varphi)}{V_{\text{th}}} \right) c_{\text{out}} \right] \quad (2.14)$$

Parameters	Value	Units
Fx_{SLCaP}	0.89	
V_{max}	2.2	$[\mu\text{mol}][\text{l}_{\text{cytosol}}]^{-1}[\text{s}]^{-1}$
K_{m}	0.5	$[\mu\text{M}]$
H	1.6	
$Q_{10\text{-SLCaP}}$	2.35	

Table 2.2: Parameters used to define the flux J_{pump} across Γ_s

Parameters	Value	Units
V_{max}	9.0	$[\mu\text{mol}][\text{l}_{\text{cytosol}}]^{-1}[\text{s}]^{-1}$
K_{mCai}	3.59	$[\mu\text{M}]$
K_{mCao}	1.3	$[\text{mM}]$
K_{mNai}	12.29	$[\text{mM}]$
K_{mNao}	87.5	$[\text{mM}]$
k_{sat}	0.27	
η	0.35	
$K_{\text{d-Act}}$	0.256	$[\mu\text{M}]$
H_{Na}	3	
Q_{NCX}	1.57	

Table 2.3: Parameters used to define the flux J_{NCX} across Γ_s

where P_{Ca} is the permeability constant for Calcium (ms^{-1}) and $\text{Be}(\cdot)$ is the inverse of the Bernoulli function, defined as

$$\text{Be}(x) = \frac{x}{e^x - 1}. \quad (2.15)$$

All these conditions are Robin boundary conditions and can be expressed in the form

$$-k_i \mathbf{f}_2 = \alpha_i c_2 - \beta_i$$

The parameters k_i , α_i and β_i are defined on each boundary of Ω_2 according to conditions (2.11), (2.12), (2.14) and (2.2f).

Chapter 3

Numerical Approximation

In this chapter we present the main numerical methods used to solve the mathematical model illustrated in Chapter 2. We start presenting the fixed point iteration used to handle the intrinsic nonlinearity of our model, namely the Gummel Map (see [6] for details and convergence analysis). Then we describe the finite element discretization procedure of the linearized problems obtained by decoupling. The adopted approach is based on domain partitioning into neighbouring blocks and employs the extension, proposed in [1], to axisymmetric geometries of the exponentially fitted stabilized scheme of [17].

3.1 Linearization methods

The system of PDEs introduced in Chapter 2, with the associated initial and boundary conditions, can not, general, be solved in closed form, hence an approximate numerical solution must be found. The partial differential model introduced is nonlinear and, to treat this difficulty, we apply a functional iteration procedure better known as Gummel Map. In this algorithm each variable of the problem and its corresponding equation are treated in sequence until convergence. We refer to

[6] for a complete description and analysis of the Gummel algorithm applied to the iterative solution of the Drift-Diffusion model for semiconductor.

The nonlinearity of our model is related to the coupling between the potential φ and the ion concentration c_i due to the drift term in the ionic flux equations (2.1b), (2.2b) and due to the nonlinear nature of the GHK model for the ionic membrane fluxes (2.14), and the other fluxes J_{SR} , J_{pump} and J_{NCX} considered as boundary conditions. Functional iterations translate the nonlinear system into a sequence of linear problems. The equations defining the potential and ion concentrations are solved separately, instead of using a monolithic algorithm. This is the Gummel Map approach and it simplifies the problem because the decoupling of the potential from the concentration variables renders the continuity equations linear and the size of the corresponding algebraic system is reduced.

3.1.1 Temporal discretization

Time dependence for the PNP system is managed by introducing a simple temporal semi-discretization. We use a Backward-Euler (BE) method to approximate all time derivatives because it is unconditionally stable, is easy to implement and introduces a time discretization error of order Δt which is of the same order as that of the discretization used for the spatial part of the differential operator. We consider the problem having a time span of $[0, T_{end}]$, T_{end} being the final time, let $t_m = m\Delta t$ the m -th time level, where $m = 0, \dots, M_T$, $M_T \geq 1$ and $\Delta t = T_{end}/M_T$. We consider $c_i^m = c_i(\mathbf{x}, t_m)$, which indicates the Calcium concentration in the domain Ω_i evaluated at the time level t_m . Using the BE method we obtain:

$$\frac{\partial c_i}{\partial t}(\mathbf{x}, t_m) \simeq \frac{c_i^{m+1}(\mathbf{x}) - c_i^m(\mathbf{x})}{\Delta t} \quad m = 0, \dots, M_T - 1$$

3.2 PNP solution map

The PNP system is formally identical to the drift diffusion model (DD) for semiconductor devices [6] and this similarity can be profitably exploited for mathematical and computational purposes. Precisely we can then apply a change of variable in such a way that expressions (2.1b), (2.2b) can be written as

$$\mathbf{f}_i = -D_i \nabla \mathbf{c}_i - z_i c_i \mu_i \nabla \varphi = -z_i D_i c_i \left(\frac{\nabla \mathbf{c}_i}{z_i c_i} + \frac{\nabla \varphi}{V_{th}} \right), \quad (3.1)$$

where we have used the Einstein relation (2.6).

It is convenient to use the definition of electrochemical potential :

$$\varphi_{ci} := \varphi + \frac{V_{th}}{z_i} \ln \frac{c_i}{c_{ref}},$$

where c_{ref} is a reference concentration, to express the ion concentration c_i as a nonlinear function of the electric and electrochemical potentials as

$$c_i = c_{ref} \exp \left(\frac{z_i (\varphi_{ci} - \varphi)}{V_{th}} \right). \quad (3.2)$$

The use of (3.2) into the Poisson equation (2.7a) has the effect of transforming the linear Poisson into a nonlinear equation. This approach is the same as done in the iterative solution of the DD system using the Gummel Map. For this reason we choose also the Gummel Map in the iterative solution of the PNP system.

At each time level t_m , the iterative procedure starts with initial guesses for the electric potential and ion concentrations, $\varphi^{(0)}$ and $c_i^{(0)}$. By indicating with (k) the generic k -th iteration, a single step of the Gummel process consists of (See Figure 3.1):

- the solution of the nonlinear Poisson equation. Using (3.2) we can rewrite

equation (2.7a) as

$$\operatorname{div}(-\epsilon \nabla \varphi) = 2qN_{av}c_{ref} \exp\left(\frac{2(\varphi_{ci} - \varphi)}{V_{th}}\right) + \rho_{fix} \quad \text{in } \Omega_i$$

and the Newton method can be applied to obtain the update potential $\varphi^{(k+1)}$. To do this we need to introduce another sub-cycle using the index j to indicate the Newton subiterations;

- the solution of the linear continuity equations for Calcium ion inside the different domains $c_i^{(k+1)}$, $i = 1, 2$, given the update potential $\varphi^{(k+1)}$ obtained in the previous step. We treat the nonlinearity, present in boundary conditions (2.1b) and (2.2f)- (2.2e), using the concentrations $c_i^{(k)}$ at the previous step, thus obtaining a linear problem to solve;
- the solution of the equation (2.5) which returns $c_{SR}^{(k+1)}$ using $c_1^{(k+1)}$ and $c_2^{(k+1)}$, computed in the previous step, to define the two fluxes \mathbf{f}_1 and \mathbf{f}_2 ;
- a check of convergence of the iteration, carried out by verifying whether the maximum absolute difference between two consecutive iterates is less than a prescribed tolerance:

$$\begin{aligned} \|\varphi^{(k+1)} - \varphi^{(k)}\|_{L^\infty(\Omega)} &< \epsilon_\varphi \\ \|c_i^{(k+1)} - c_i^{(k)}\|_{L^\infty(\Omega)} &< \epsilon_c \quad i = 1, 2, \text{SR} \end{aligned} \quad (3.3)$$

where we set, for a measurable function f

$$\|f\|_{L^\infty(\Omega)} = \inf \{M \geq 0 : |f| \leq M \text{ almost everywhere in } \Omega\}$$

3.2.1 The Nonlinear Poisson equation

Each step of the Gummel Map for the PNP system requires solving a nonlinear Poisson equation to update the potential $\varphi^{(k+1)}$. This corresponds to finding the zero of the operator

$$F(\varphi) = -\lambda^2 \operatorname{div} \nabla \varphi - \rho_{fix} - 2 \exp \left(\frac{2(\varphi_{ci} - \varphi)}{V_{th}} \right), \quad (3.4)$$

We solve the nonlinear PDE

$$F(\varphi) = 0 \quad \text{in each } \Omega_i \quad i = 1, 2$$

supplied by suitable boundary and interface conditions. A solution can be obtained by applying the Newton method, a fixed point iteration which consists in solving at each step j , $j \leq 0$, until convergence, the following linearized problem

$$\begin{aligned} F'(\varphi^{(j)}) \delta\varphi^{(j)} &= -F(\varphi^{(j)}) \\ \varphi^{(j+1)} &= \varphi^{(j)} + \delta\varphi^{(j)} \end{aligned} \quad (3.5)$$

where $F'(\varphi^{(j)})$ is the Fréchet derivative of F , evaluated at $\varphi^{(j)}$ and acting in a linear manner on the increment function $\delta\varphi^{(j)}$.

3.2.2 Continuity equations

Once the electric potential $\varphi^{(k+1)}$ is determined by iteratively solving the NLP equations as illustrated in Sect.3.2.1, the next step of the Gummel map consists of the solution of the linear continuity equation for Calcium ions in the two subdomain Ω_1 and Ω_2 with linear boundary and interface conditions. The boundary problems to be solved to determine the updated ion concentrations $c_1^{(k+1)}$ and $c_2^{(k+1)}$ for each subdomain Ω_i , $i = 1, 2$, read as follows:

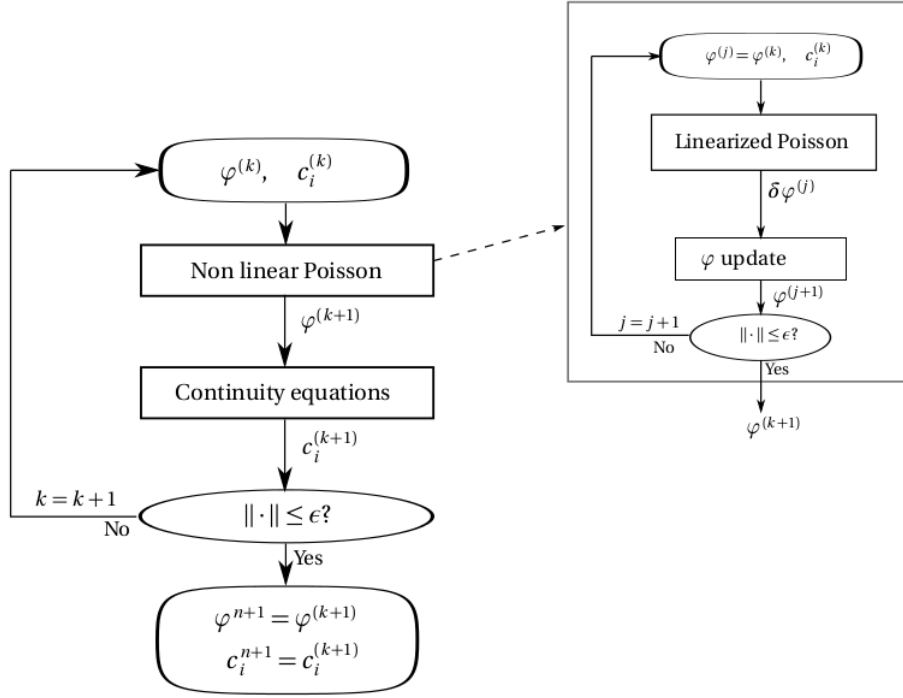


Figure 3.1: PNP solution map

$$\frac{c_i^{(k+1)}}{\Delta t} + \operatorname{div} \mathbf{f}_i(c_i^{(k+1)}, \varphi^{(k+1)}) = \frac{c_i^m}{\Delta t} \quad \text{in } \Omega_i \quad (3.6a)$$

$$\mathbf{f}_i(c_i^{(k+1)}, \varphi^{(k+1)}) = -D \nabla c_i^{(k+1)} - z c_i^{(k+1)} \mu \nabla \varphi^{(k+1)} \quad (3.6b)$$

$$-k_j \mathbf{f}_i \cdot \mathbf{n}_j + \alpha_j c_i^{(k+1)} = \beta_j \quad \text{on } \partial \Omega_i \quad (3.6c)$$

All the boundary conditions chosen for our model are linearized taking the value of c_i at the previous step of the algorithm when we define the coefficients α_j and β_j in (3.6c), as already described in Section 2.2.1, and using the value of c_{SR} computed at the previous time step.

The last step of the Gummel map computes $c_{\text{SR}}^{(k+1)}$ as the solution of the equation (2.5), which is equivalent to solving:

$$\frac{\mathbf{c}_{\text{SR}}^{(k+1)}}{\Delta t} = \frac{\mathbf{c}_{\text{SR}}^{(m)}}{\Delta t} + P_{\text{SR}} \left(\mathbf{c}_1^{(k+1)}, \mathbf{c}_2^{(k+1)}, \mathbf{c}_{\text{SR}}^{(k+1)} \right) \quad (3.7)$$

where $P_{\text{SR}} \left(\mathbf{c}_1^{(k+1)}, \mathbf{c}_2^{(k+1)}, \mathbf{c}_{\text{SR}}^{(k+1)} \right)$ depends on $\mathbf{c}_1^{(k+1)}$ and $\mathbf{c}_2^{(k+1)}$, already computed in the previous step of the Gummel Map. A schematic representation of the complete algorithm is shown in Figure 3.1.

3.3 Spatial discretization

In the present work we study a geometrical configuration where the domain Ω is partitioned in two subdomains Ω_1 and Ω_2 , such that $\Omega = \Omega_1 \cup \Omega_2$, $\Gamma = \partial\Omega_1 \cap \partial\Omega_2$ and $\partial\Omega = (\partial\Omega_1 \cup \partial\Omega_2) \setminus \Gamma$, in which we have to solve the system of PDEs (See Figure 3.2). We consider the following advective-diffusive model boundary value problem:

$$\operatorname{div} \mathbf{j}_i = f_i \quad \text{in } \Omega_i, i = 1, 2 \quad (3.8a)$$

$$\mathbf{j}_i = -\mu_i \nabla \mathbf{u}_i + \mathbf{v}_i \mathbf{u}_i \quad \text{in } \Omega_i, i = 1, 2 \quad (3.8b)$$

$$\llbracket \mathbf{j} \cdot \mathbf{n} \rrbracket_{\Gamma} = \mathbf{j}_1 \cdot \mathbf{n}_1 + \mathbf{j}_2 \cdot \mathbf{n}_2 = \sigma \quad \text{on } \Gamma \quad (3.8c)$$

$$\llbracket \mathbf{u} \rrbracket_{\Gamma} = \mathbf{u}_2 - \mathbf{u}_1 = g \quad \text{on } \Gamma \quad (3.8d)$$

$$k_i \mathbf{j}_i \cdot \mathbf{n}_i = \alpha_i \mathbf{u}_i - \beta_i \quad \text{on } \partial\Omega \quad (3.8e)$$

In order to write the weak formulation for the two problems we define the

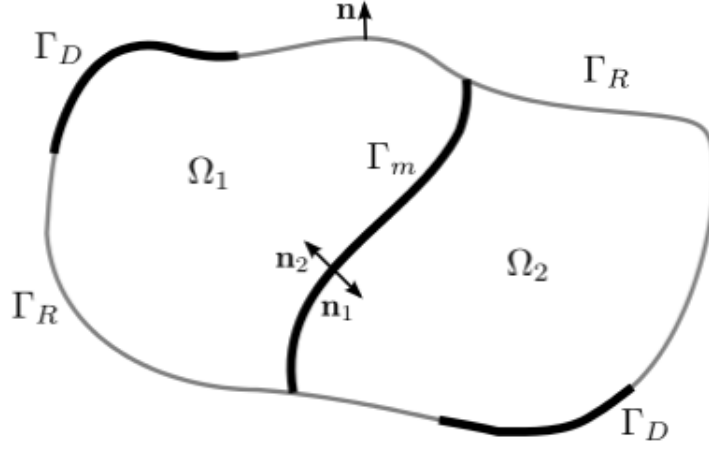


Figure 3.2: Partition of the computational domain Ω into two different but communicating parts

functional spaces

$$\begin{aligned}
 V &:= H^1(\Omega) \\
 V_i &:= H^1(\Omega_i) \quad \text{for } i = 1, 2 \\
 \Lambda &:= \{\omega \in H^{\frac{1}{2}}(\Gamma) : \omega = v|_{\Gamma} \text{ for a suitable } v \in V\}
 \end{aligned} \tag{3.9}$$

so that our problem becomes: find $u_i \in V_i$, $i = 1, 2$, such that:

$$- \int_{\Omega_i} \mathbf{j}_i \cdot \nabla v_i + \int_{\partial\Omega_i \setminus \Gamma} v_i \mathbf{j}_i \cdot \mathbf{n}_i + \int_{\Gamma} v_i \mathbf{j}_i \cdot \mathbf{n}_i = \int_{\Omega_i} f_i v_i \quad \forall v_i \in V_i \tag{3.10}$$

Let us introduce the bilinear forms

$$a_{\Omega_i}(u_i, v_i) = - \int_{\Omega_i} \mathbf{j}_i \cdot \nabla v_i \, d\Omega_i$$

and the linear functionals

$$F_{\Omega_i}(\mathbf{v}_i) = \int_{\Omega_i} f_i \mathbf{v}_i \, d\Omega_i - \int_{\partial\Omega_i \setminus \Gamma} \mathbf{j}_i \cdot \mathbf{n}_i \mathbf{v}_i \, ds_i$$

Problem (3.10) is the same as: find $\mathbf{u}_i \in U_i$ such that

$$a_{\Omega_i}(\mathbf{u}_i, \mathbf{v}_i) = F_{\Omega_i}(\mathbf{v}_i) \quad \forall \mathbf{v}_i \in V_i \quad (3.11a)$$

$$\mathbf{u}_2|_{\Gamma} - \mathbf{u}_1|_{\Gamma} = g \quad (3.11b)$$

$$\sum_{i=1}^2 a_{\Omega_i}(\mathbf{u}_i, R_i\phi) + F_{\Omega_i}(R_i\phi) = \sigma \quad \forall \phi \in \Lambda \quad (3.11c)$$

where $R_i\phi$ is an extension of $\phi \in \Lambda$ to U_i .

We note that, if we apply the above method to the Poisson problem (2.7), σ is equal to $-\sigma_{\text{SR}}$, $\mathbf{v}_i = 0 \, \forall i = 1, 2$ and $g = 0$ from equations (2.7g) and (2.7h).

Now introduce a spatial discretization of equations (3.11a) - (3.11c); to this purpose we use piecewise linear finite elements on a regular triangulation T_h^i of each of the two subdomains Ω_i such that

$$\Omega_i = \bigcup_{K \in T_h^i} K$$

with the following properties

- $\text{int}(K) \neq \emptyset$;
- $\text{int}(K_1) \cap \text{int}(K_2) = \emptyset$ for each distinct $K_1, K_2 \in T_h^i$;
- if $F = K_1 \cap K_2 \neq \emptyset$, with K_1 and K_2 distinct elements of T_h^i , then F is a common edge or vertex of K_1 and K_2 ;

- $\text{diam}(K) \leq h \forall K \in T_h^i$.

Then we consider the following subspaces of V_i and Λ :

$$V_i^h := X_h^1(\Omega_i) \cap V_i = \{v_h \in C^0(\overline{\Omega_i}) : v_h|_{K_i} \in \mathbb{P}_1(K_i) \forall K_i \in T_h^i\} \cap V_i$$

$$\Lambda^h := \{\omega \in H^{\frac{1}{2}}(\Gamma) : \omega = v|_{\Gamma} \text{ for a suitable } v \in X_h^1\}$$

Now we are able to write the discretized form of system (3.12a) - (3.12c), obtaining:

$$a_{\Omega_i}^h(\mathbf{u}_h^i, \mathbf{v}_h^i) = F_{\Omega_i}(\mathbf{v}_h^i) \quad \forall \mathbf{v}_h^i \in V_i^h \quad (3.12a)$$

$$\mathbf{u}_h^2|_{\Gamma} - \mathbf{u}_h^1|_{\Gamma} = g \quad (3.12b)$$

$$\sum_{i=1}^2 a_{\Omega_i}^h(\mathbf{u}_h^i, R_h^i \phi) + F_{\Omega_i}(R_h^i \phi) = \sigma_h \quad \forall \phi \in \Lambda^h \quad (3.12c)$$

where the approximate bilinear form $a_{\Omega_i}^h$ replace the form a_{Ω_i} by using the method proposed in [17] and recently extended to axisymmetric geometries in [1].

At this stage it is possible to write the algebraic system associated with the above problem. For each subdomain, we define

$$\mathbf{u}^i = \begin{bmatrix} \mathbf{u}_I^i \\ \mathbf{u}_{\Gamma}^i \end{bmatrix}$$

where \mathbf{u}_I^i denotes the vector of internal unknowns of each subdomain, \mathbf{u}_{Γ}^i collects

the unknowns belonging to Γ . Therefore for every subdomain we have

$$A^i \begin{bmatrix} \mathbf{u}_I^i \\ \mathbf{u}_\Gamma^i \end{bmatrix} = \begin{bmatrix} \mathbf{f}_I^i \\ \mathbf{f}_\Gamma^i \end{bmatrix} + M^i \begin{bmatrix} 0 \\ \mathbf{H}_\Gamma^i \end{bmatrix} \quad (3.13)$$

where the block \mathbf{H}_Γ represents the fluxes across Γ . The matrix A^i is the discretization form of $a_{\Omega_i}(\cdot, \cdot)$ and is defined as

$$A^i = \begin{bmatrix} A_{II}^i & A_{I\Gamma}^i \\ A_{\Gamma I}^i & A_{\Gamma\Gamma}^i \end{bmatrix} \quad (3.14)$$

while

$$M^i = \begin{bmatrix} 0 & 0 \\ 0 & M_{\Gamma\Gamma}^i \end{bmatrix} \quad (3.15)$$

is a sparse block matrix accounting for the quadrature rule adopted when computing the integrals on the right hand side of (3.12a)-(3.12c). We also obtain $M_{\Gamma\Gamma}^1 = M_{\Gamma\Gamma}^2$ because of the conformity of the two grids over Γ .

Finally the interface conditions are:

$$\mathbf{u}_\Gamma^2 - \mathbf{u}_\Gamma^1 = g \quad (3.16a)$$

$$\mathbf{H}_\Gamma^1 + \mathbf{H}_\Gamma^2 = -\sigma_h \quad (3.16b)$$

Chapter 4

Numerical simulations and results

In this chapter we present the numerical results obtained with the application of the numerical methods of Chapter 3 to the mathematical models illustrated in Chapter 2.

We implemented the numerical models using Octave, an open-source language, because of the availability of computer codes developed in previous works for the generation of meshes (Octave package `msh`) and for the construction of the matrices resulting from the spatial discretizations using radial and cylindrical coordinates (package `bim`). As we have already discussed in Chapter 3 we linearized the problems using the Gummel Map in which the Newton subcycle is dealt with the nonlinear solver `fsolve`. The tolerances (3.3) for the most of the simulations are set to as $\epsilon_\varphi \simeq 10^{-9}$ and $\epsilon_c \simeq 10^{-6}$.

4.1 Stationary simulations

In order to test the mathematical model proposed in Chapter 2 we start with stationary simulations in the two dimensional geometry, illustrated in Fig. 2.4, with cylindrical coordinates. We consider a cross section in the $r - z$ plane,

so that we are actually investigating the three dimensional problem, thanks to the symmetry with respect to the ϕ -coordinate. The boundary conditions for this model are represented in Fig. 2.4 and described in detail in Chapter 2.

- on Γ_{sym} we impose homogeneous Neumann conditions on both potential and concentrations, as required by the axial symmetry;
- on Γ_s we impose a Robin boundary condition for the concentration, using the linearized form of equation (2.2f) and a homogeneous Neumann condition for the potential;
- on Γ_l and Γ_r we choose again a Robin condition for the concentration, based on the GHK equation, and for the potential, in which we take into account the presence of the cell membrane with its capacitance c_m ;
- on Γ_{SR} we have the SR membrane on which we have to solve the equation (2.5) and we impose Robin conditions both on Ω_1 and Ω_2 for the concentrations and the transmission conditions (2.7f) and (2.7g) for the potential.

The mesh used in the numerical simulations is shown in Fig. 4.1, the red part correspond to the subdomain Ω_2 , while the blue part is the subdomain Ω_1 . We set $R = 10 \mu\text{m}$ and $Z = 100 \mu\text{m}$ which correspond to the cell radius and the cell length respectively and the depth of the subdomain Ω_2 corresponds to the subsarcolemma radius, $R_{\text{SL}} = 0.45 \mu\text{m}$.

4.1.1 Models for Calcium in the sarcoplasmic reticulum

In this section we have to model P_{SR} , the reaction term of the equation (2.5). The first choice we consider is to express this reaction term as an interfacial flux

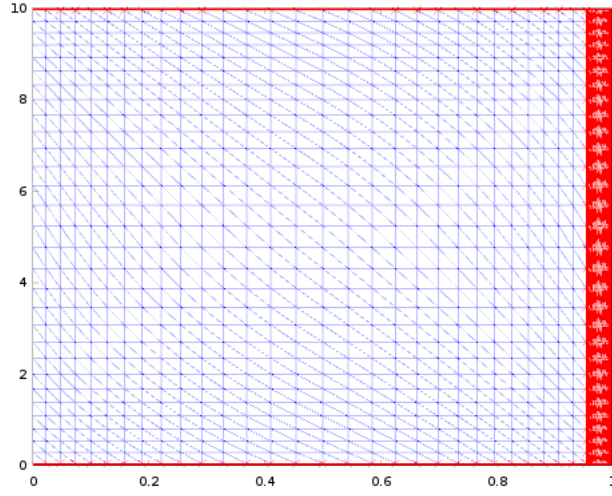


Figure 4.1: Mesh for the axisymmetric geometry of Fig.2.2: the blue grid represents the subdomain Ω_1 , the red represents Ω_2 .

given by the sum of the two fluxes coming from the subdomains Ω_1 and Ω_2

$$P_{\text{SR}} = \frac{1}{t_{\text{SR}}} (\mathbf{f}_1 \cdot \mathbf{n}_1 + \mathbf{f}_2 \cdot \mathbf{n}_2) \quad (4.1)$$

Because of the expression of the two fluxes, given by equations (2.1b) and (2.2b), which are dependent on c_1 , c_2 and c_{SR} we can consider the right hand side term, P_{SR} , as a jump condition as illustrated in [16].

We consider the static case, assuming

$$\frac{\partial c_i}{\partial t} = 0 \quad i = 1, 2, \text{SR}$$

so the equation for c_{SR} becomes

$$P_{\text{SR}} = 0 \quad \text{on } \Gamma_{\text{SR}} \quad (4.2)$$

Parameters	Value	Units
D_{Ca}	$1.5 * 10^{-10}$	$[m^2][s^{-1}]$
P_{Ca}	5.4	$[\mu m][s^{-1}]$
c_{out}	1	$[mM]$
V_{out}	0	$[V]$
$[K]_i$	140	$[mM]$
$[K]_o$	5	$[mM]$
$[Na]_i$	4	$[mM]$
$[Na]_o$	145	$[mM]$
$[Cl]_i$	144	$[mM]$
$[Cl]_o$	150	$[mM]$

Table 4.1: Environmental parameters

and using the discretization form of equation (4.1) we obtain

$$c_{SR}^{(k+1)} = g \left(c_1^{(k+1)}, c_2^{(k+1)}, c_{SR}^{(k)} \right)$$

where g is a nonlinear function of the three variables computed in the previous steps of the Gummel Map. The parameters used for this simulation are listed in Tables 2.1, 2.2, 2.3 and 4.1.

The results are shown in Figures 4.2, 4.3 and 4.6.

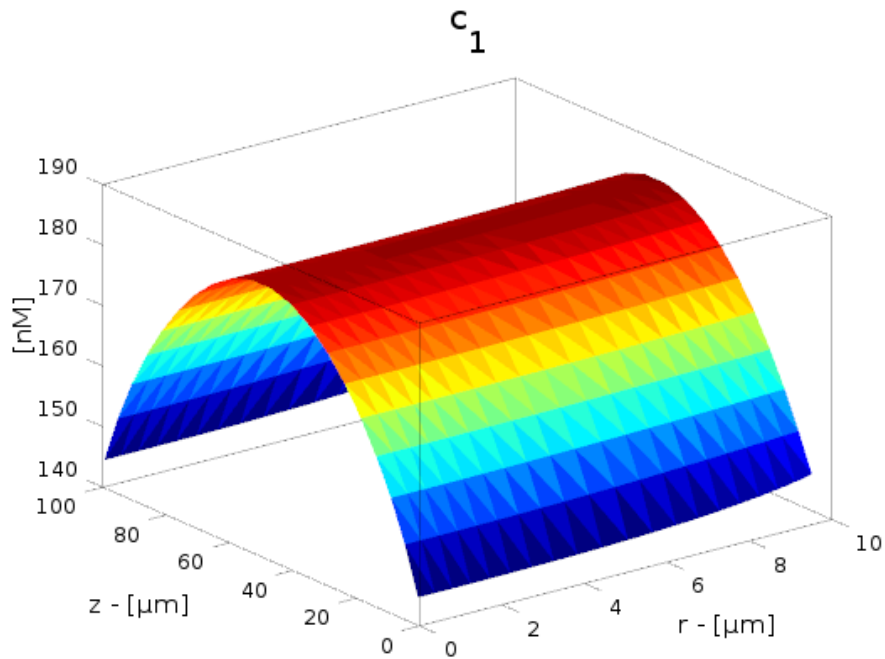
We compute the mean value of Calcium concentration in each subdomain, in Ω_1 we have $\bar{c}_1 = 172.76nM$ which is comparable with experimental results. The concentration in Ω_2 is higher, $\bar{c}_2 = 1.1848mM$, and this result is in agreement with [13], because there are spatial gradients near the SL membrane which are likely due to diffusion restrictions. Finally we can observe that the mean value of Calcium concentration in the sarcoplasmic reticulum is $\bar{c}_{SR} = 1.1856mM$. We expect higher concentration of Calcium in the SR than in the cytosol and in the subsarcolemma, because the SR works as a Calcium store. For this reason we have decided to improve model (4.1) for the net production rate P_{SR} . The idea is to consider a simplified model in which P_{SR} is linearly dependent on

the concentrations of the three subdomains:

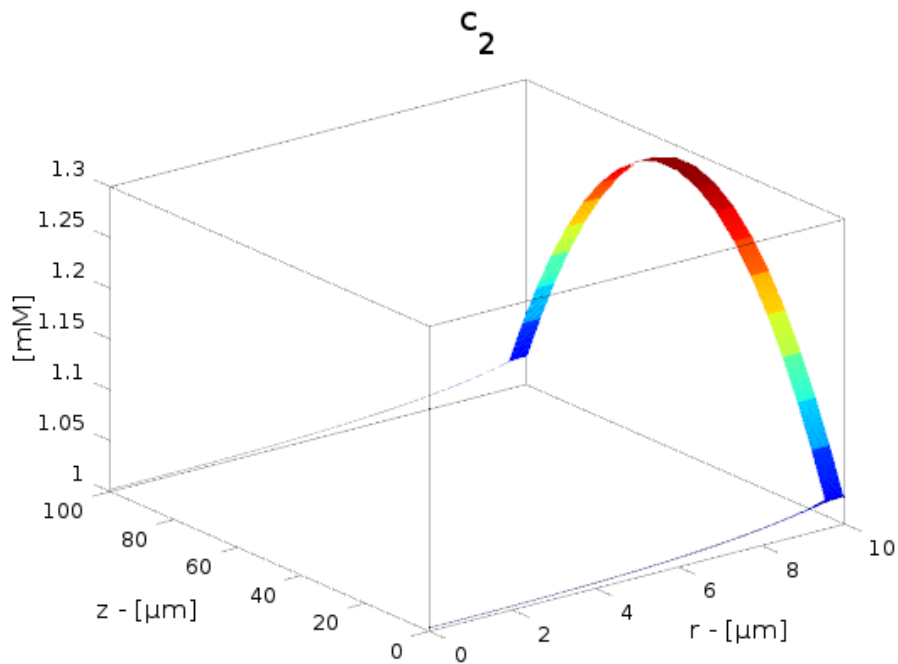
$$P_{\text{SR}} = c_{\text{SR}} - (m_1 c_1 + m_2 c_2) \quad (4.3)$$

where m_1 and m_2 are constant variables such that $m_1, m_2 \geq 0$ and $m_2 \leq 1$. We fix the value of $m_2 = 0.9$ and we increase the value of m_1 ranging from 600 to 800. We estimate these value starting from the nonlinear conditions imposed in the previous simulation. The value of \bar{c}_1, \bar{c}_2 and \bar{c}_{SR} with the change of m_1 are listed in Table 4.2. We can observe that the distance between the concentrations c_{SR} and c_2 increases with m_1 , see Figure 4.6, but beyond a certain value of this parameter the two concentrations become too high, for this reason we believe that in the first place the best choice for m_1 is $m_1 = 740$. Simulations obtained with this value of m_1 are shown in Figures 4.4 and 4.5. We can observe that the concentration profile of c_{SR} follows the trend of c_2 due to the values of the two parameters m_1 and m_2 , but in this model the difference between the two concentrations increases. The values of the concentrations are higher, however are still in good agreement with the experimental results, in particular, as regards the difference between the cytosolic concentration and the subsarcolemma concentration.

The intracellular potential (see Figure 4.7) resulting from this simulation is (almost) null because of the electroneutrality condition imposed at each step of the algorithm and because of the absence of concentration gradients in agreement with the constant value of the extracellular concentration. Figure 4.8 shows the two component of the fluxes \mathbf{f}_1 and \mathbf{f}_2 over the two subdomain. We can observe that the r -component of the flux is continuous on the upper interface, while the z -component is continuous on the side edges. This is due to the fact that parameters m_1 and m_2 are chosen starting from the model (4.1) in which the continuity between the two fluxes along Γ_{SR} is required.



(a) Calcium concentration in the cytosol



(b) Calcium concentration in the SL

Figure 4.2: Calcium concentration in the domains Ω_1 and Ω_2 computed using model (4.1) for the SR

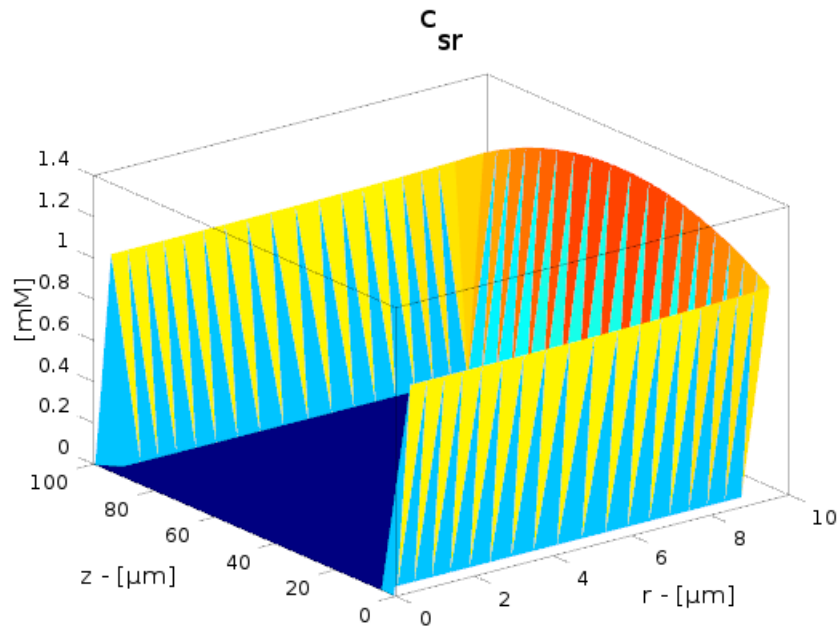


Figure 4.3: Calcium concentration in the sarcoplasmic reticulum computed using model (4.1) for the SR

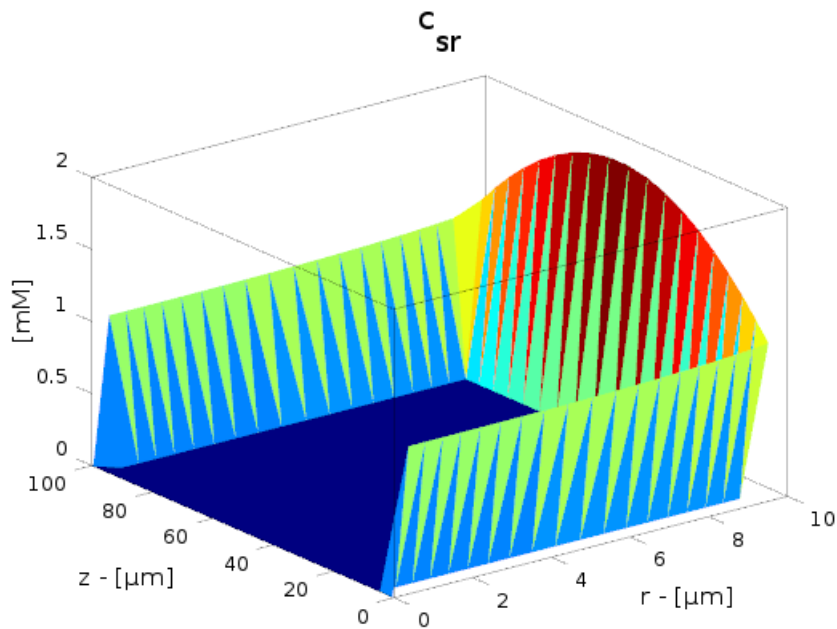
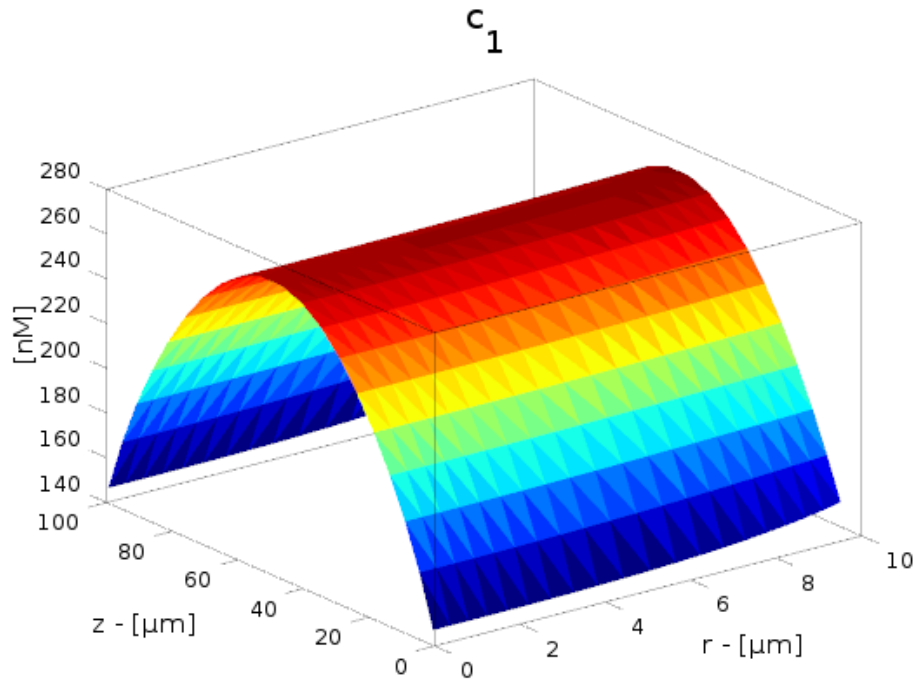
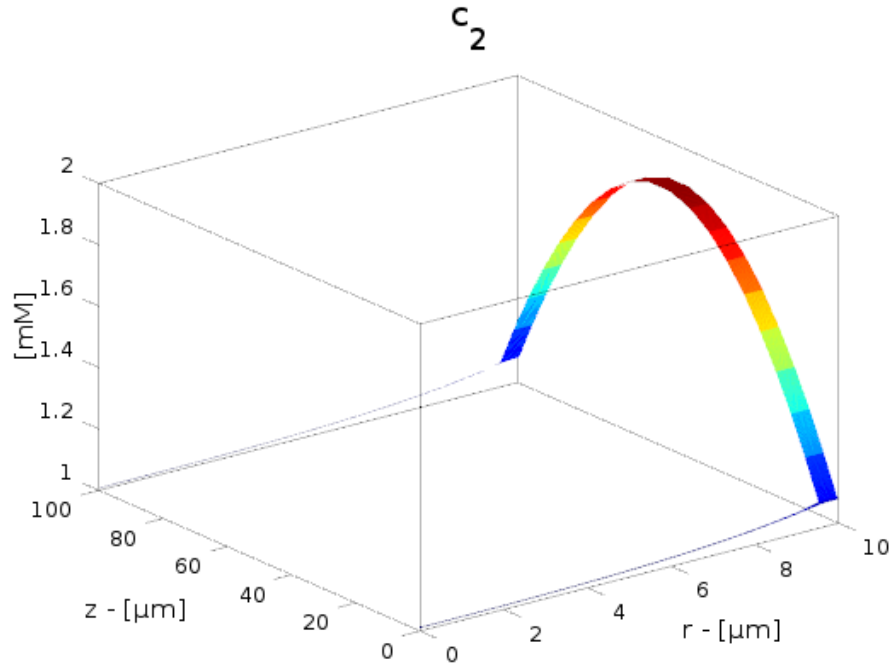


Figure 4.4: Calcium concentration in the sarcoplasmic reticulum computed using model (4.3) for the SR and setting $m_1=740$ and $m_2=0.9$



(a) Calcium concentration in the cytosol



(b) Calcium concentration in the SL

Figure 4.5: Calcium concentration in the domains Ω_1 and Ω_2 computed using model (4.3) for the SR and setting $m_1=740$ and $m_2=0.9$

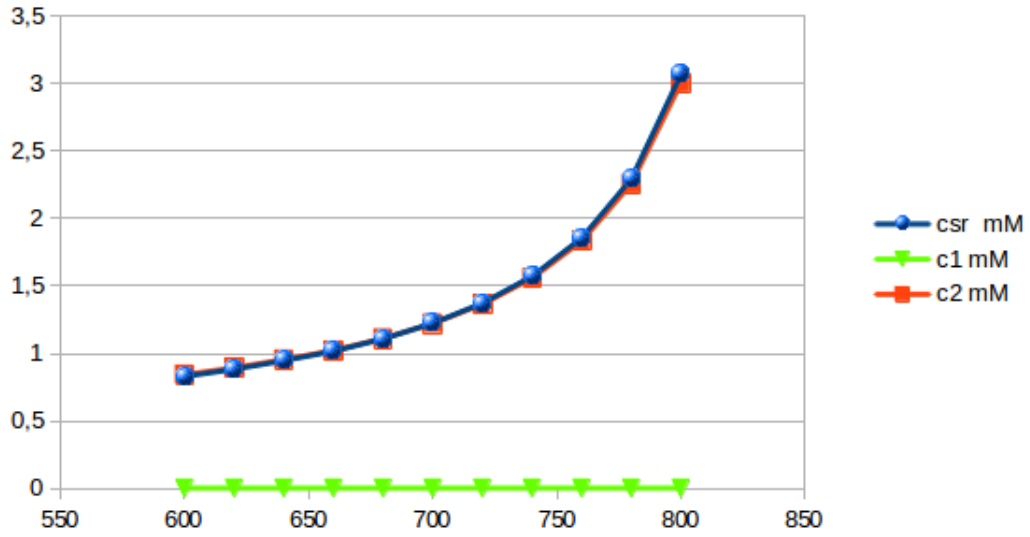


Figure 4.6: Concentrations trend due to the variation of the parameter m_1

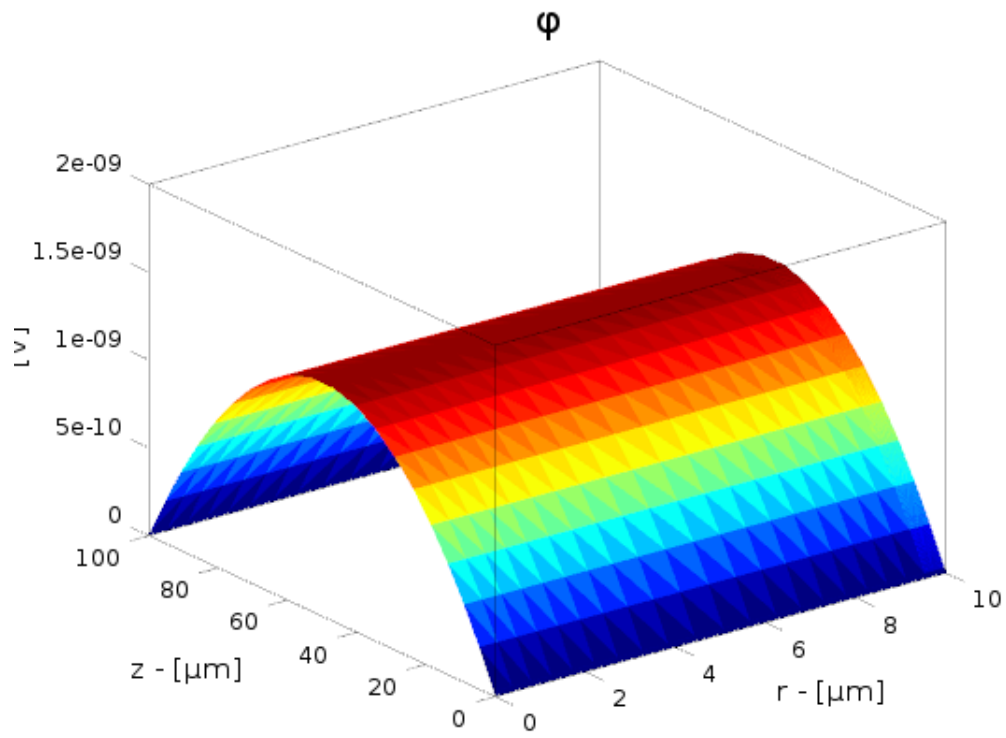
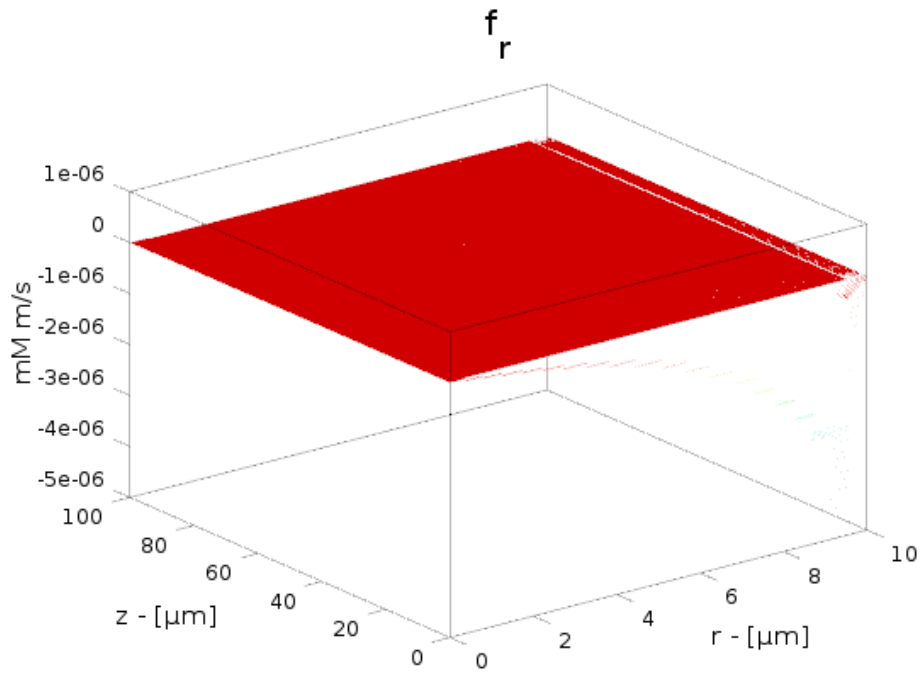
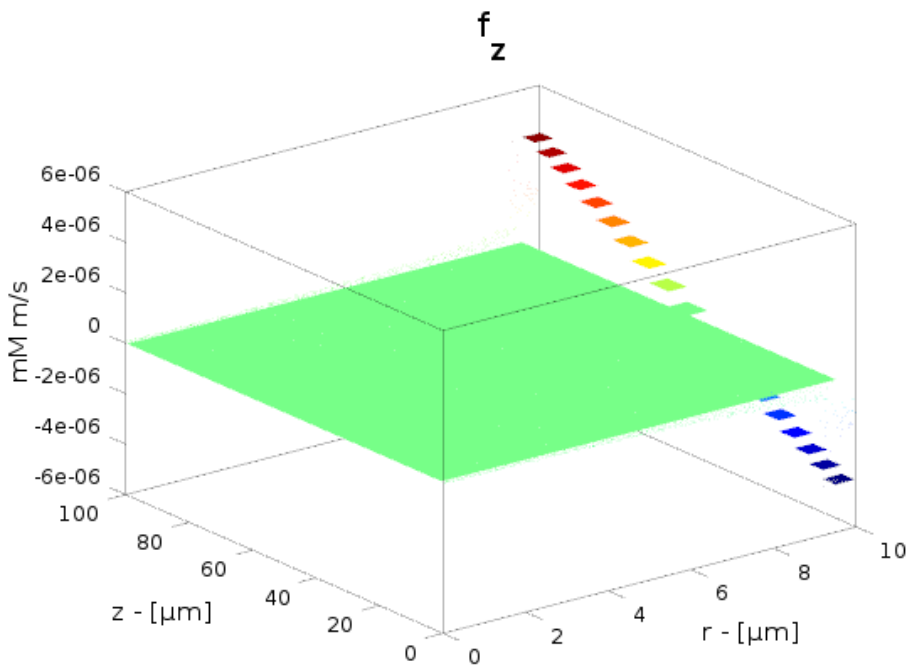


Figure 4.7: Intracellular potential



(a) Flux component in the r -direction



(b) Flux component in the z -direction

Figure 4.8: Component of the two fluxes f_1 and f_2 computed using model (4.3) for the SR and setting $m_1=740$ and $m_2=0.9$

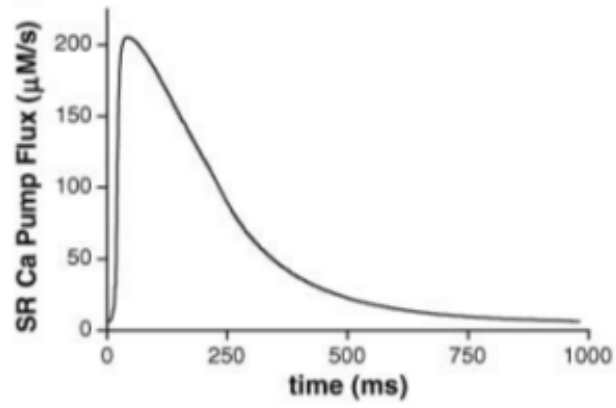
m_1	\bar{c}_1 [nM]	\bar{c}_2 [mM]	\bar{c}_{SR} [mM]
600	117.97	0.8424	0.8292
620	126.23	0.894	0.8830
640	135.98	0.9549	0.94658
660	146.74	1.0221	1.0166
680	160.93	1.1108	1.1088
700	178.69	1.2219	1.2241
720	201.56	1.3654	1.373
740	232.53	1.5586	1.5731
760	276.45	1.8334	1.8574
780	344.26	2.258	2.2963
800	464.04	3.0081	3.0709

Table 4.2: Calcium average concentrations in the three subdomains following the variation of the parameter m_1

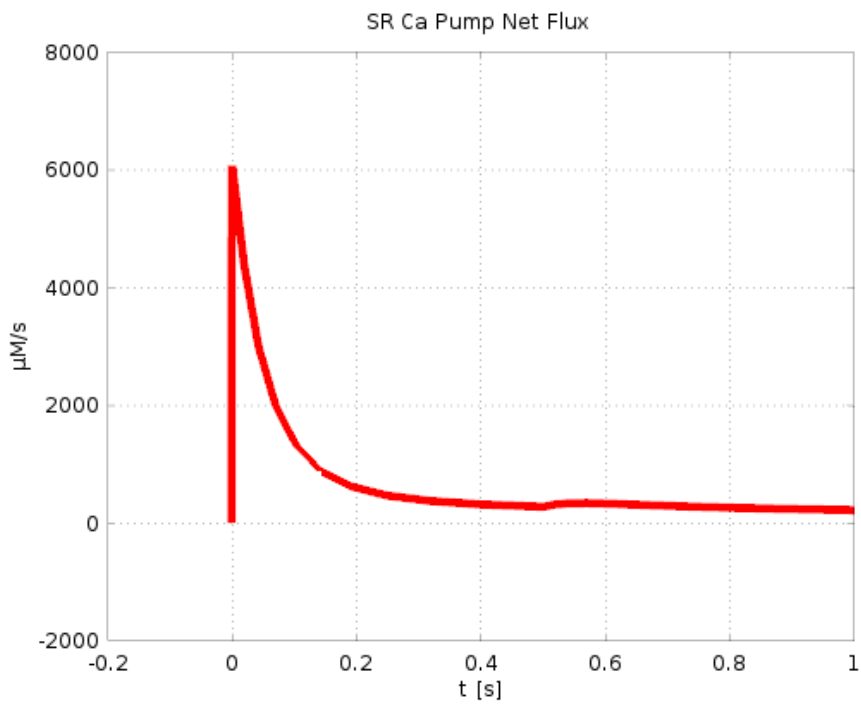
4.2 Time dependent simulations

In the previous section we have proposed and numerically validated two models for the stationary behaviour of the SR. Starting from these simulations we introduce the temporal dependence in the continuity equations (2.1a), (2.2a) in order to reproduce some results shown in [13]. We simulate the behaviour of the membrane channels, in particular the SR Ca pumps and the Na-Ca exchangers. We vary the intracellular potential from -60 to $+40$ mV and we start computing the behaviour of the SR Calcium pumps. The SR Ca pump formulation is the same as in [13] and pumps are modeled as a reversible enzyme, mediating both "forward" and "reverse" unidirectional fluxes. The net flux into the SR is the difference between these latter fluxes. The net transport rate from the cytosol to the SR rises during the release as cytosolic Calcium rises and SR Calcium falls. This causes a tendency for the pump to operate in the forward mode, transporting more Calcium into the SR. The resulting flux is shown in Figure 4.9.

The qualitative behaviour of the SR Ca pumps is the same as in [13] with a



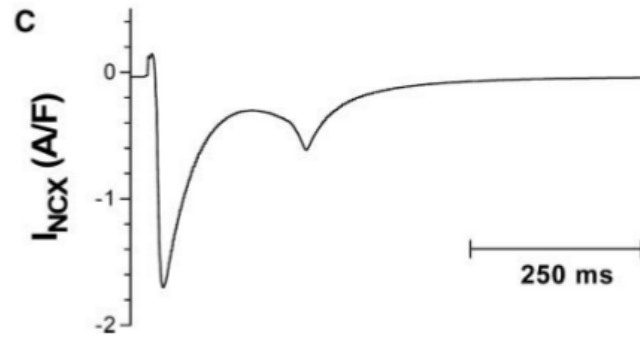
(a) Shannon et al. [13]



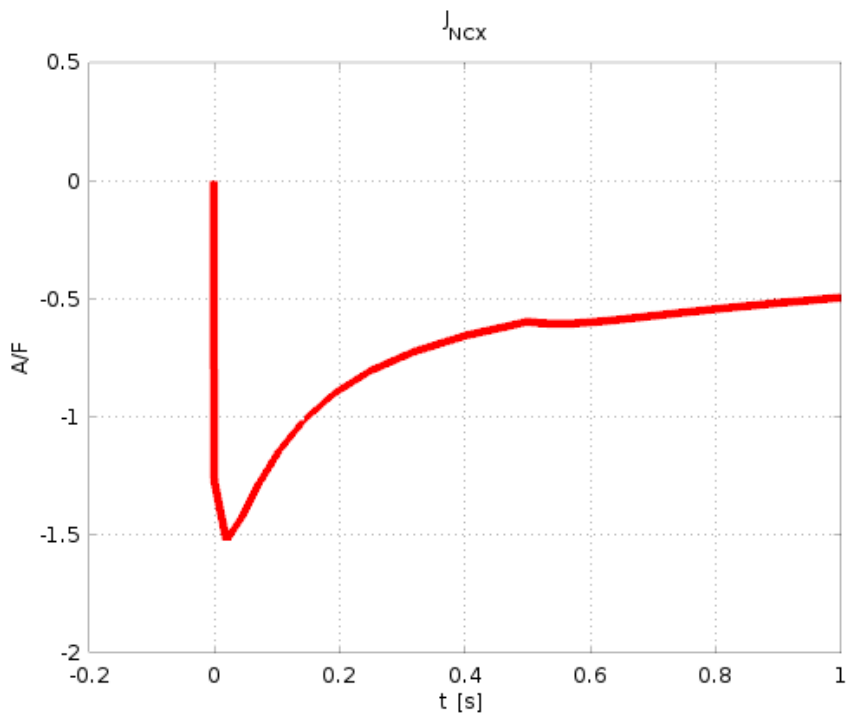
(b) Model simulation

Figure 4.9: Net SR Ca pump flux

higher value of the peak in our simulated profile. The other important component of this model are the Na-Ca exchangers and the subsarcolemma Ca pumps which transport Calcium from the subsarcolemma to the extracellular compartment. The formulation of the Na-Ca exchanger, based on [13], accounts for the dependence on Calcium concentrations in the subsarcolemma and on intracellular Na concentration. The results of the simulation of this flux are shown in Figure 4.10 and are qualitatively comparable with the results from [13]. It is important to notice that in our formulation the Na dynamics is neglected because we consider the other ions as a fixed charge, as described in Chapter 2.



(a) Shannon et al. [13]



(b) Model simulation

Figure 4.10: Na-Ca exchangers flux

Chapter 5

Conclusions and Future Work

In the present Master Thesis we have proposed and numerically implemented a mathematical model for the simulation of Calcium dynamics inside a cardiac myocyte. We have introduced a new geometrical representation of the intracellular space which accounts the main compartments that characterize the intracellular environment. On this geometry we have developed suitable boundary and interface conditions for the mathematical model in order to simulate the behaviour of ion channels located on cellular membranes. Numerical simulations show the spatial distribution of Calcium inside the different compartments and the resulting fluxes across the cell membrane and the SR interface. Even if the present work is far from a real world description, it can be considered as a first important step for the construction of a sound mathematical model to be used in the Calcium dynamics simulation. Future research is needed to provide a better description of this very complex phenomenon. An important improvement for this model is the inclusion of the spatial dynamics of the other ions involved in Calcium dynamics, such as Na^+ , K^+ and Cl^- , which have been incorporated in the present work just considering them as fixed charges. Another possible development is to model in a more complex and realistic manner the dynamics of Calcium in the sarcoplasmic

reticulum appropriately determining the spatial dynamics of the concentration in this organelle. These future improvements should give the realistic chance to go further in the study of the dynamics of Calcium and other ions inside the cell and in the description of the excitation-contraction coupling triggered by them.

Appendix A

The PNP system in scaled form

In this section we reformulate the mathematical system introduced in Section 2.2 in order to obtain a scaled set of equations, where variables are adimensional and normalized. This operation, called scaling, is very useful in view of numerical computations, since the variables of the problem may have physical values of very different magnitude.

We introduce the following independent scaling factors: \bar{r} , \bar{c} , $\bar{\varphi}$ and \bar{D} , and we set:

$$\bar{r} = \text{diam}(\Omega)$$

$$\bar{c} = \max_{i=1,2} \left\{ c_i^{(in)}, c_i^{(out)} \right\}$$

$$\bar{\varphi} = V_{th}$$

$$\bar{\mu} = \max_{i=1,2} \{ \mu_i \}$$

We start by scaling equations (2.1a), (2.1b) and (2.2a), (2.2b) and obtain

$$\frac{\bar{c}}{\bar{t}} \frac{\partial \widehat{c}_i}{\partial \widehat{t}} + \frac{1}{\bar{r}} \widehat{\text{div}} \mathbf{f}_i = 0$$

$$\mathbf{f}_i = z \mu \bar{c} \hat{E} \hat{\mathbf{E}} - D \frac{\widehat{\nabla} \hat{c}_i}{\bar{r}} \bar{c}$$

Using the Einstein relation (2.6) and introducing the scaling factor for the electric field $\bar{E} = \frac{\bar{\varphi}}{\bar{r}}$ we obtain:

$$\mathbf{f}_i = z \mu \frac{\bar{c} \bar{\varphi}}{\bar{r}} \hat{E} \hat{\mathbf{E}} - \frac{\mu V_{th} \bar{c}}{|z| \bar{r}} \widehat{\nabla} \hat{c}_i$$

Setting $\bar{\varphi} = V_{th}$ we get

$$\begin{aligned} \mathbf{f}_i &= \bar{\mu} \bar{E} \bar{c} \frac{z}{|z|} \left(|z| \widehat{\mu} \hat{c}_i \hat{\mathbf{E}} - z \widehat{\nabla} \hat{c}_i \right) \\ &= \bar{f} s \left(|z| \widehat{\mu} \hat{c}_i \hat{\mathbf{E}} - z \widehat{\nabla} \hat{c}_i \right) \end{aligned} \tag{A.1}$$

where we define the scaling factor for the flux density

$$\bar{f} = \bar{\mu} \bar{E} \bar{c}$$

and $s =: \text{sign}(z)$.

Thus we obtain the scaled flux density

$$\hat{\mathbf{f}}_i = z \widehat{\mu} \hat{c}_i \hat{\mathbf{E}} - |z| \widehat{\nabla} \hat{c}_i$$

and replacing this expression in the continuity equation we get the scaling factor for the time variable

$$\bar{t} = \frac{\bar{r}}{\bar{\mu} \bar{E}}.$$

Finally we have to treat the boundary conditions of the two problems, which

have the expression

$$-k\mathbf{f}_i \cdot \mathbf{n}_i = \alpha c_i - \beta$$

. Proceeding as done before we obtain:

$$\widehat{\mathbf{f}}_i = \frac{\bar{c}}{f} \alpha \widehat{c}_i - \frac{\beta}{f} = \widehat{\alpha} \widehat{c}_i - \widehat{\beta}$$

where the scaled quantities $\widehat{\alpha}$ and $\widehat{\beta}$ are expressed as:

$$\widehat{\alpha} = \frac{\alpha}{\bar{\mu} \bar{E}}$$

$$\widehat{\beta} = \frac{\beta}{f}$$

Then we get the following system of scaled equations:

$$\begin{aligned} \frac{\partial \widehat{c}_i}{\partial t} + \widehat{\mathbf{div}} \widehat{\mathbf{f}}_i &= 0 && \text{in } \Omega_i \\ \widehat{\mathbf{f}}_i &= z \widehat{\mu} \widehat{c}_i \widehat{\mathbf{E}} - |z| \widehat{\nabla} \widehat{c}_i && \\ \widehat{\mathbf{f}}_i \cdot \mathbf{n} &= 0 && \text{on } \Gamma_{\text{sym}} \cap \partial \Omega_i \\ \widehat{\mathbf{f}}_i &= \widehat{\alpha} \widehat{c}_i - \widehat{\beta} && \text{on } \partial \Omega_i \end{aligned} \tag{A.2}$$

The scaling of the Poisson equation (2.7a) gives

$$\frac{\varepsilon_0 \bar{\varphi}}{qr^2 \mathbf{N}_{\text{av}} \bar{c}} \widehat{\mathbf{div}} \left(-\varepsilon_r \widehat{\nabla} \widehat{\varphi} \right) = 2 \widehat{c}_i + \sum_{j=1}^M z_j c_j$$

from which, introducing the adimensional parameter

$$\lambda^2 := \frac{\bar{\varphi} \varepsilon_w}{r^2 q \mathbf{N}_{\text{av}} \bar{c}}$$

we obtain the following scaled form

$$-\lambda^2 \widehat{\text{div}} \widehat{\nabla} \widehat{\varphi} = 2\widehat{c}_i + \widehat{\rho}_{fix}$$

We now consider the equation (2.7d) (the same treatment can be done for condition (2.7e))

$$\widehat{\mathbf{D}} \cdot \mathbf{n}_l = \frac{c_m \bar{\varphi} \bar{r}}{\varepsilon_0 \bar{\varphi}} (\widehat{\varphi} - \widehat{V}_l)$$

Defining the scaling factor for the membrane capacitance

$$\bar{c}_m = \frac{\varepsilon_0}{\bar{r}}$$

we obtain the scaled boundary condition

$$\widehat{\mathbf{D}} \cdot \mathbf{n}_l = \widehat{c}_m (\widehat{\varphi} - \widehat{V}_l)$$

Ringraziamenti

Desidero ringraziare tutti coloro che mi hanno aiutato nella realizzazione della mia Tesi. Ringrazio il professor Riccardo Sacco per avermi dato la possibilità di lavorare su questo interessante argomento, per la sua disponibilità e il suo aiuto nell'affrontare questo tema complesso e nuovo nell'ambito della ricerca. Un grande ringraziamento anche a Matteo Porro per la sua continua disponibilità nonostante tutti i suoi impegni e alla professoressa Paola Causin per il contributo fondamentale nella stesura del modello.

In primo luogo vorrei ringraziare la mia famiglia che mi ha sostenuto moralmente ed economicamente per tutti questi anni universitari. Grazie a loro ho potuto intraprendere questo percorso e con il loro sostegno e i loro incoraggiamenti sono riuscita a portarlo a termine. Grazie a mia nonna che mi sosteneva durante gli esami con le sue preghiere nonostante la mia poca fede.

Un ringraziamento speciale va a tutti i miei compagni, per le interminabili giornate di studio trascorse insieme, per le feste e le serate che hanno reso questo lungo e faticoso percorso universitario più leggero e pieno di esperienze uniche. Ho incontrato persone speciali che saranno un ricordo indelebile nella mia vita. Un grazie particolare a Cristina con cui ho potuto condividere le maggiori gioie e i maggiori dolori di questo percorso, sempre presente e sempre pronta a incorag-

giarmi, con le serate al Biraus e le interminabili code in tangenziale alla mattina. Ringrazio Francesca per tutti gli anni di convivenza insieme in cui mi buttava giù dal letto e mi faceva comunque arrivare tardi a lezioni, per essermi stata accanto nei, non pochi, momenti difficili di questi anni e per tutto il supporto psicologico che non ha mai smesso di darmi neppure a distanza. Grazie ai PECE che hanno reso l'ultimo anno universitario uno dei migliori della mia vita, in particolare a Paola che mi è sempre stata vicina e sarà sempre una persona su cui potrò contare nonostante la distanza fisica che ci separa e a Ema per tutte le risate e tutti i maltrattamenti che mi ha regalato in questi anni. Ringrazio Luigi per avermi aiutato sia nello studio che nei miei problemi e nelle mie ansie con l'infinita pazienza che lo contraddistingue.

Un grazie particolare a tutti i miei amici della Brianza per i week end spensierati che mi tenevano per un poco lontano dal Poli.

In ultimo, ma sicuramente uno dei più importanti, un grazie a Luca che mi è stato vicino per tutto questo travagliato e a volte anche difficile periodo di tesi con tutto l'affetto e il sostegno possibile.

Bibliography

- [1] E. Abbate. “Hierarchical Multiscale Modeling and Simulation of Bio-Electronic Interfaces”. Tesi di laurea. Politecnico di Milano, 2012/2013.
- [2] L. Bursztyn et al. “Mathematical model of excitation-contraction in a uterine smooth muscle cell”. In: *Am. J. Physiol., Cell Physiol.* 292.5 (2007), pp. C1816–1829.
- [3] A. Cangiani and R. Natalini. “A spatial model of cellular molecular trafficking including active transport along microtubules”. In: *J. Theor. Biol.* 267.4 (2010), pp. 614–625.
- [4] G. Bard Ermentrout and David H. Terman. *Mathematical Foundations of Neuroscience*. 1st Edition. Springer, 2010.
- [5] D. D. Friel and H. J. Chiel. “Calcium dynamics: analyzing the Ca²⁺ regulatory network in intact cells”. In: *Trends Neurosci.* 31.1 (2008), pp. 8–19.
- [6] J.W. Jerome. *Analysis of Charge Transport: A Mathematical Study of Semiconductor Devices*. Ed. by Springer Verlag. New York, 1996.
- [7] A. Kapela, A. Bezerianos, and N. M. Tsoukias. “A mathematical model of Ca²⁺ dynamics in rat mesenteric smooth muscle cell: agonist and NO stimulation”. In: *J. Theor. Biol.* 253.2 (2008), pp. 238–260.

- [8] A. Kapela and N. M. Tsoukias. “Multiscale FEM modeling of vascular tone: from membrane currents to vessel mechanics”. In: *IEEE Trans Biomed Eng* 58.12 (2011), pp. 3456–3459.
- [9] J. P. Keener and J. Sneyd. *Mathematical Physiology*. New York: Springer, 1998.
- [10] D. Rossi et al. “The sarcoplasmic reticulum: an organized patchwork of specialized domains”. In: *Traffic* 9.7 (2008), pp. 1044–1049.
- [11] I. Rubinstein. *Electrodifussion of Ions*. Philadelphia, PA: SIAM, 1990.
- [12] T. R. Shannon, F. Wang, and D. M. Bers. “Regulation of cardiac sarcoplasmic reticulum Ca release by luminal [Ca] and altered gating assessed with a mathematical model”. In: *Biophys. J.* 89.6 (2005), pp. 4096–4110.
- [13] T. R. Shannon et al. “A mathematical treatment of integrated Ca dynamics within the ventricular myocyte”. In: *Biophys. J.* 87.5 (2004), pp. 3351–3371.
- [14] G. D. Smith et al. “A simple numerical model of calcium spark formation and detection in cardiac myocytes”. In: *Biophys. J.* 75.1 (1998), pp. 15–32.
- [15] C. A. Walker and F. G. Spinale. “The structure and function of the cardiac myocyte: a review of fundamental concepts”. In: *J. Thorac. Cardiovasc. Surg.* 118.2 (1999), pp. 375–382.
- [16] S. Whitaker. “The species mass jump condition at a singular surface”. In: *Chemical Engineering Science* 47.7 (1991), pp. 1667–1685.
- [17] J. Xu and L. Zikatanov. “A monotone finite element scheme for convection–diffusion equations”. In: *Math. Comp.* 68(228) (1999), pp. 1429–1446.